2009

Efficient Cone Beam Reconstruction For The Distorted Circle And Line Trajectory

Souleymane Konate
University of Central Florida

EFFICIENT CONE BEAM RECONSTRUCTION FOR THE DISTORTED CIRCLE AND LINE TRAJECTORY

by

SOULEYMANE KONATE
B.S. Universite Dakar-Bourguiba, 2000
M.S. University Central Florida, 2004

A dissertation submitted in partial fulfillment of the requirements
for the degree of Doctor of Philosophy
in the Department of Mathematics
in the College of Sciences
at the University of Central Florida
Orlando, Florida

Spring Term
2009

Major Professor: Alexander Katsevich

ABSTRACT

We propose an exact filtered backprojection algorithm for inversion of the cone beam data in the case when the trajectory is composed of a distorted circle and a line segment. The length of the scan is determined by the region of interest , and it is independent of the size of the object. With few geometric restrictions on the curve, we show that we have an exact reconstruction. Numerical experiments demonstrate good image quality.

To my parents Moussa Konate and Aisse Traore

ACKNOWLEDGMENTS

Thanks to all the people who directly or indirectly supported me in this endeavor.

TABLE OF CONTENTS

LIST OF FIGURES viii

LIST OF TABLES x

CHAPTER ONE: INTRODUCTION 1

CHAPTER TWO: RADON TRANSFORM AND ITS INVERSION FORMULA . . . 4

2.1 Definition of the Radon Transform 4

2.2 The Fourier Slice Theorem 6

2.3 3–D Radon Inversion Formula 7

CHAPTER THREE: THE CONE BEAM TRANSFORM 10

3.1 Definition of the Cone Beam Transform 10

3.2 Relation between the Cone Beam Transform and the Radon Transform . . . 10

CHAPTER FOUR: GENERAL SCHEME FOR CONSTRUCTING INVERSION ALGORITHMS FOR CONE BEAM CT 14

4.1 General Definitions 14

4.2 Conditions on the trajectory 15

4.3 Katsevich's General Inversion Formula 16

CHAPTER FIVE: THE CIRCLE AND LINE ALGORITHM 22

5.1 Introduction and General Settings 22

5.2 Katsevich's Inversion Formula for the Circle and Line Trajectory 25

CHAPTER SIX: THE DISTORTED CIRCLE AND LINE ALGORITHM 31

6.1 Motivation and Research Outline 31

6.2 Class of Curves 32
6.3 The Distorted Circle 40
6.3.1 Existence and Smoothness of R(s) 40
6.3.2 Choice of R(s) and its Consequence 44
6.3.3 The Pi Line and its Properties 44
6.3.4 Projection on the Detector Plane DP(s) 50
6.4 Weight Distribution and Inversion Theorem 55
CHAPTER SEVEN: THE ALGORITHM AND ITS IMPLEMENTATION 57
7.1 Description of the Cone Beam (CB) Measurements 57
7.1.1 General Formulation 57
7.1.2 Flat Detector Geometry 58
7.2 Katsevich Formula 62
7.2.1 Filtering 63
7.2.2 Backprojection 63
7.3 Numerical Implementation Strategies 64
7.3.1 Filtering 64
7.3.2 Backprojection 71
CHAPTER EIGHT: NUMERICAL RESULTS 74
LIST OF REFERENCES 78

LIST OF FIGURES

2.1 The Radon Transform in $\mathbb{R}^2$ 5

3.1 The Cone Beam Transform 11

4.1 Illustration of the Weight Function 17

4.2 Illustration of the Normalization Condition 18

5.1 Circle and Line Trajectory 23

5.2 Projection when the source is located on the line 26

5.3 Projection when the source is located on the line 27

5.4 Projection when the source is located on the circle 29

6.1 Illustration of the convexity with respect to y(0) 33

6.2 Illustration of Lemma 3 35

6.3 Illustration of the Proof of Lemma 3 36

6.4 Illustration of the Proof of Lemma 4 38

6.5 Illustration of Lemma 5 39

6.6 Existence of the Function $R(s)$ 43

6.7 Existence and Smoothness of $R(s)$ 45

6.8 $R(0) - R(s)\cos(s) > 0$ 46

6.9 Violation of the Convexity w.r.t the origin $y(0)$ 49

6.10 Illustration of Lemma 11 52

7.1 Ideal and Distorted Circle 59

7.2 Flat Detector Geometry 61

7.3 Filtering when the source is on the Circle 67

7.4 Illustration of the Height of the Cylindrical ROI 68

7.5 Filtering when the source is on the Line 69

7.6 Filtering when the source is on the Line (Interpolation) 70

7.7 Backprojection 72

7.8 Bilinear Interpolation prior to Backprojection 73

8.1 Cross section $z = 20$ mm through the reconstructed clock phantom. The region $|x| \leq 250$,$|y| \leq 250$ mm is show for a distortion parameter of $\epsilon = 5.0$. 76

LIST OF TABLES

6.1 Definition of the Weight Function $n(s, x, \alpha)$ 55

8.1 HU of Some Common Substances 75

8.2 Simulation and Reconstruction Parameters 77

CHAPTER ONE: INTRODUCTION

In practice, Computer Tomography (CT) is one of the most powerful tools in medical imaging. The equipment utilizes x-rays produced from different angles. In case of a trauma, CT can help locate multiple organs injuries. Additionally, it can be used to confirm the presence of lesions such as cysts, solid tumors, and to determine the extent to which other organs are affected.

From a scientific prospective, there is a complicated process that lead to the visualization of these images. As a rough explanation, line integrals are obtained by sending an x-ray beam through the human body. By inverting the resulting line integrals, one can reconstruct the x-ray attenuation coefficient inside of the body. In practice, the attenuation coefficient allows experts to make conclusions about the inner structure of the body. From a mathematical standpoint, let us consider a beam of x-ray propagating through a medium. In our case, the body of the patient represents the medium. Assume the velocities of the x-ray particles are the same, and they are equal to v. Additionally, assume the collision between the particles is neglected. The particles may collide with the fixed atoms of the medium, and in this case, they are absorbed, provided the scattering is null.

Let $\psi = \psi(x,t)$ be the density of the particles at the spatial location x and at the time t. Then the transport equation is the differential form of the conservation of particles law:

$$\frac{\partial \psi(x,t)}{\partial t} + v \cdot \nabla \psi = -|v|\sigma(x)\psi(x,t) + q(x,t), \tag{1.1}$$

where $q(x,t)$ is the source term, and $\sigma(x)$ is the probability of absorption of the particle at the point (x,t). Let $v = |v|\alpha$, where α is the unit vector in the direction of v, and let $x = x_0 + s\alpha$, be the parametric equation of the line L along which the particles propagate. If one considers the stationary case, then equation (1.1) becomes

$$\frac{\partial\psi(x)}{\partial s} = -\sigma(x)\psi(x) + h(x),\ x = x_0 + s\alpha \tag{1.2}$$

In this case, $h = q/|v|$; it is assumed that $|v|$ is constant and positive, and the source term is independent of α. In x-ray transmission, $\psi := I$ represents the intensity of the x-ray beam, $h(x) = 0$ means there are no sources of the radiation inside of the body, and $\sigma := f$ is the x-ray attenuation coefficient, proportional to the density of the body. So (1.2) becomes

$$\frac{dI(x)}{ds} = -f(x)I(x),\ x = x_0 + s\alpha. \tag{1.3}$$

By integrating both sides of the equation along the line L,

$$\frac{I}{I_0} = \exp\Big(-\int_L f(x)dx\Big), \tag{1.4}$$

where I_0 is the initial intensity of the beam before entering the body, and I is the intensity of the beam registered by the detector upon exit of the body. Therefore,

$$\ln\frac{I_0}{I} = \int_L f(x)dx, \tag{1.5}$$

Since I_0 is known, from the observed quantity I, one can determine the line integral of f. In this problem, the attenuation coefficient is the unknown. The CT problem is to reconstruct the coefficient f given the set of its line integrals. This is where an exact inversion formula is needed in order to convert the data collected from the scanners into images.

CHAPTER TWO: RADON TRANSFORM AND ITS INVERSION FORMULA

2.1 Definition of the Radon Transform

Let f be a function in $\mathbb{R}^n$, which is integrable over all hyperplanes in $\mathbb{R}^n$. The Radon transform integrates the function f over hyperplanes. It is defined as follows:

$$\hat{f}(\alpha, p) = \int_{H(\alpha,p)} f(x)dx, \ \alpha \in S^{n-1}, \tag{2.1}$$

where S^{n-1} is the unit sphere in $\mathbb{R}^n$, and $H(\alpha, p) = \{x : x \cdot \alpha = p, \alpha \in S^{n-1}\}$ is an hyperplane in $\mathbb{R}^n$.

As an example, figure 2.1 gives an illustration of the Radon transform in 2–D. In $\mathbb{R}^2$, $H(\alpha, p)$ is a line. The directional vector corresponding to α is $(\cos\alpha, \sin\alpha) \in S^1$. The Radon transform of the function f i.e $\hat{f}(\alpha, p)$ is the line integral of f along the line $H(\alpha, p)$. Even though $\hat{f}(\alpha, p)$ is defined for $p \geq 0$, it can be extended to an even function due the fact that $H(-\alpha, -p) = H(\alpha, p)$. Other notations are

$$\hat{f}(\alpha, p) = \int_{\mathbb{R}^n} f(x)\delta(p - x \cdot \alpha)dx, \tag{2.2}$$

where δ is the Dirac Delta function, and

$$\hat{f}(\alpha, p) = \int_{\alpha^\perp} f(x + p\alpha)dx, \tag{2.3}$$

where

$$\alpha^\perp = \{x \in R^n : x \cdot \alpha = 0\}. \tag{2.4}$$

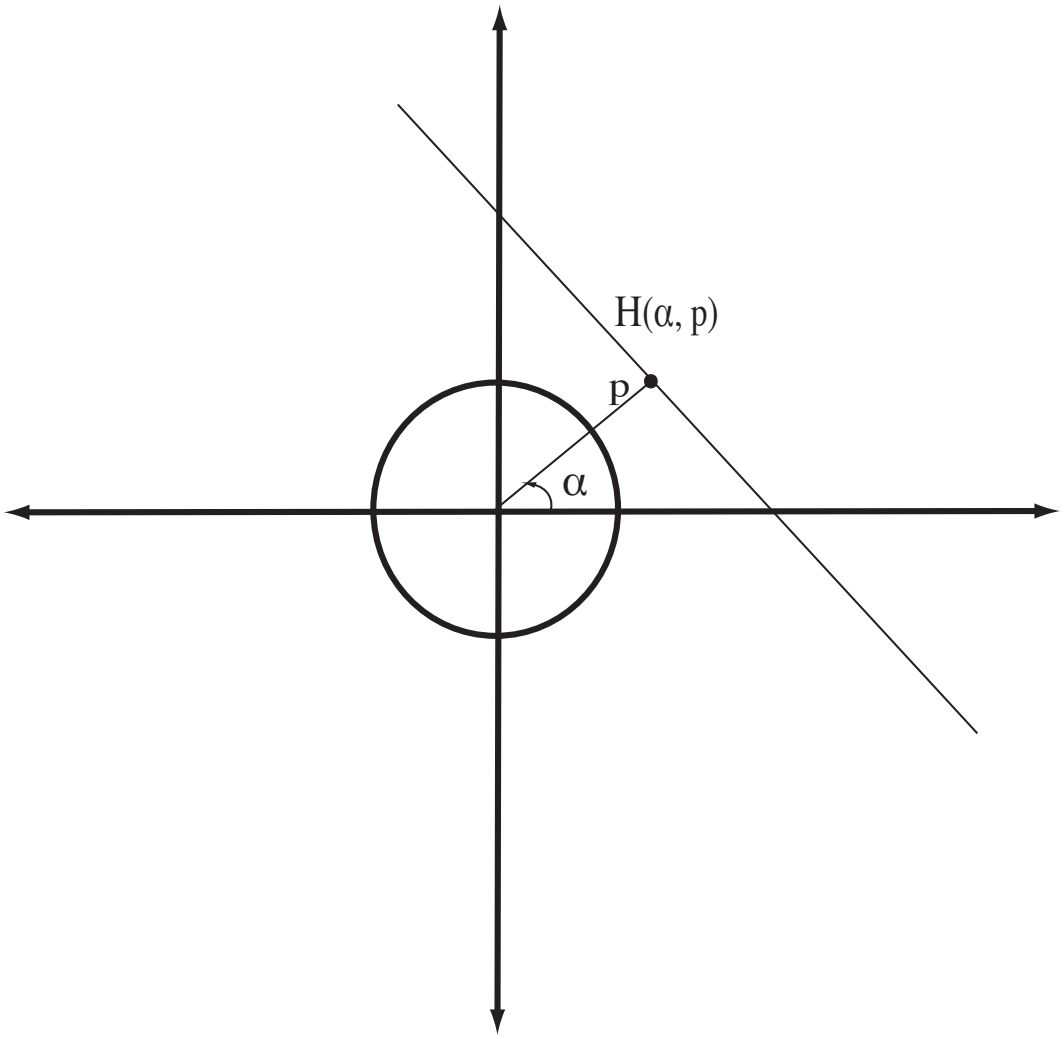

Figure 2.1: The Radon Transform in $\mathbb{R}^2$

2.2 The Fourier Slice Theorem

Let us introduce the Fourier transform. The Fourier transform of a function, denoted $\tilde{f}$, is defined as :

$$\tilde{f}(y) := \mathcal{F}[f](y) := \int_{\mathbb{R}^n} f(x) \exp(ix \cdot y) dx. \tag{2.5}$$

The inverse Fourier transform is given by the following formula:

$$\mathcal{F}^{-1}[\tilde{f}](y) := \frac{1}{(2\pi)^n} \int_{\mathbb{R}^n} f(x) \exp(-ix \cdot y) dx. \tag{2.6}$$

Theorem 1 (Fourier Slice Theorem) *Let $\mathcal{F}_p$ denote the one dimensional Fourier transform with respect to the second argument. Then for $\alpha \in S^{n-1}, t \in \mathbb{R}$,*

$$\mathcal{F}_{p \to t}[\hat{f}] := \int_{-\infty}^{\infty} \hat{f}(\alpha, p) \exp(ipt) dp = \tilde{f}(t\alpha), \tag{2.7}$$

where

$$\tilde{f}(t\alpha) := (\mathcal{F}f)(t\alpha) := \int_{\mathbb{R}^n} f(x) e^{it\alpha \cdot x} dx. \tag{2.8}$$

Proof:

$$\begin{aligned} \mathcal{F}_p[\hat{f}](\alpha, t) &= \int_{-\infty}^{\infty} \exp(ipt) \int_{\mathbb{R}^n} f(x) \delta(p - \alpha \cdot x) dx dp \\ &= \int_{\mathbb{R}^n} f(x) \int_{-\infty}^{\infty} \delta(p - \alpha \cdot x) \exp(ipt) dp dx \\ &= \int_{\mathbb{R}^n} \exp(it\alpha \cdot x) f(x) dx \\ &= \tilde{f}(t\alpha) \end{aligned} \tag{2.9}$$

■

One can also show that the Radon transform of a convolution of two functions is the convolution of the Radon transforms:

$$\mathcal{R}[f * g](\omega, p) = \hat{f}(\omega, p) * \hat{g}(\omega, p). \tag{2.10}$$

Whereas the convolution on the left hand side is n-dimensional, the one on the right hand side is one dimensional, and it is performed with respect to the second argument.

2.3 3–D Radon Inversion Formula

Define $\mathcal{C}_0^\infty(\mathbb{R}^3)$ to be the set of smooth and compactly supported functions defined on $\mathbb{R}^3$. If we assume that $f \in \mathcal{C}_0^\infty(\mathbb{R}^3)$, then by using the Fourier Slice Theorem, f can be computed in the following manner:

$$f = \mathcal{F}^{-1}\mathcal{F}f = \mathcal{F}^{-1}\mathcal{F}_p\hat{f} = \mathcal{F}^{-1}\mathcal{F}_p\mathcal{R}f. \tag{2.11}$$

If f is compactly supported, then so is $\mathcal{R}f$. If $f \in \mathcal{C}_0^\infty(\mathbb{R}^3)$, then $\mathcal{R}f \in \mathcal{C}_0^\infty(S^2 \times \mathbb{R})$. Thus, $\mathcal{F}_p\mathcal{R}f$ is a well defined function of $t\alpha$. Therefore, $\mathcal{F}^{-1}\mathcal{F}_p\mathcal{R}f$ is well-defined.

Theorem 2 *3–D Radon Inversion Formula*

For every $x \in \mathbb{R}^3$,

$$f(x) = -\frac{1}{8\pi^2}\int_{S^2}\frac{\partial^2}{\partial p^2}\hat{f}(\alpha, p)|_{p=\alpha\cdot x}d\alpha. \tag{2.12}$$

PROOF: Using the first equation in (2.11),

$$f = \mathcal{F}^{-1}\mathcal{F}_{p\to t}\hat{f}. \tag{2.13}$$

In other words we have the following,

$$f(x) = \frac{1}{(2\pi)^3} \int_{\mathbb{R}^3} d\alpha \exp(-it\alpha \cdot x) \int_{-\infty}^{\infty} dp \exp(itp) \hat{f}(\alpha, p). \tag{2.14}$$

By using spherical coordinates, we have

$$f(x) = \frac{1}{8\pi^3} \int_{S^2} d\alpha \int_0^{\infty} dt\ t^2 \exp(-it\alpha \cdot x) \int_{-\infty}^{\infty} dp \exp(itp) \hat{f}(\alpha, p) \tag{2.15}$$

$$= \frac{1}{8\pi^3} \int_{S^2} d\alpha \int_{-\infty}^{\infty} dp \hat{f}(\alpha, p) \int_0^{\infty} dt\ t^2 \exp\Big(- it(p - \alpha \cdot x)\Big) \tag{2.16}$$

From [10], we can recall the following identities:

$$\int_0^{\infty} t^{n-1} e^{its} dt = i^n (n-1)! s^{-n} + (-i)^{n-1} \pi \delta^{n-1}(s) \tag{2.17}$$

Also recall that the function $\hat{f}(\alpha, p)$ is even, and $1/(p - \alpha x)^n$ is odd for $n = 3$, so in the sense of distributions [10],

$$\int_{S^n} \int_{-\infty}^{\infty} \frac{\hat{f}(\alpha, p)}{(p - \alpha \cdot x)^n} dp d\alpha = 0, \text{ for } n = 3. \tag{2.18}$$

By using (2.17) and (2.18), we obtain the following

$$\begin{aligned} f(x) &= -\frac{1}{8\pi^2} \int_{S^2} \int_{-\infty}^{\infty} \hat{f}(\alpha, p) \delta''(p - \alpha \cdot x) dp d\alpha \\ &= -\frac{1}{8\pi^2} \int_{S^2} \hat{f}''(\alpha, p = \alpha \cdot x) dp d\alpha, \end{aligned} \tag{2.19}$$

since for a compactly supported function ϕ,

$$\int_{-\infty}^{\infty} \phi(x)\delta^{(n)}(x - x_0)dx = (-1)^n \phi^{(n)}(x - x_0). \tag{2.20}$$

This ends the proof of the Radon inversion formula in $\mathbb{R}^3$. ■

CHAPTER THREE: THE CONE BEAM TRANSFORM

3.1 Definition of the Cone Beam Transform

Let f be a compactly supported C^1 function in $\mathbb{R}^3$. Provided that f is integrable over any straight line in $\mathbb{R}^3$, then the cone beam is defined to be the set of all integrals over all straight lines in $\mathbb{R}^3$. Let $y \in \mathbb{R}^3$ be a point on the line l, and θ be a vector in the unit sphere S^2. Note that θ is the direction of the ray emanating from the point y. Then the cone beam transform of f denoted by $g(y, \theta)$ is given by:

$$g(y, \theta) := \int_0^\infty f(y + t\theta)dt, y \in \mathbb{R}^3, \theta \in S^2. \tag{3.1}$$

3.2 Relation between the Cone Beam Transform and the Radon Transform

In practice, the data actually measured allows the computation of the cone beam transform of the x-ray attenuation coefficient f. It is theoretically easier to invert the Radon transform than it is to invert the cone beam transform. This is the main reason why it is necessary to find a relation between the two transforms. The following lemma relates the cone beam transform and the Radon transform in $\mathbb{R}^n$.

Lemma 1 *Let k be a distribution on $\mathbb{R}$ and $f \in \mathcal{C}_0^\infty(\mathbb{R}^n)$. Suppose that k is positively*

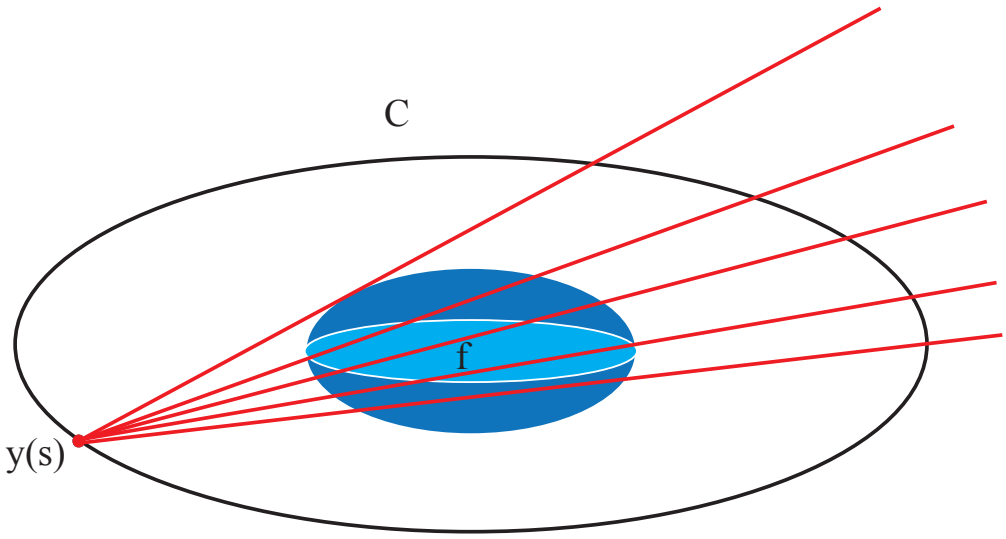

Figure 3.1: The Cone Beam Transform

homogeneous of degree $1-n$ *i.e*

$$k(ts) = t^{1-n}k(s),\ t > 0. \tag{3.2}$$

Then one has the following:

$$\int_{\mathbb{R}} \hat{f}(\alpha, p)k(p - \alpha \cdot y)dp = \int_{S^{n-1}} g(y, \theta)k(\alpha \cdot \theta)d\theta \tag{3.3}$$

Proof:

$$\begin{aligned}
\int_{S^{n-1}} g(y,\theta)k(\alpha\cdot\theta)d\theta &= \int_{S^{n-1}}\int_0^\infty f(y+t\theta)t^{1-n}k(\alpha\cdot\theta)t^{n-1}dtd\theta && (3.4)\\
&= \int_{S^{n-1}}\int_0^\infty f(y+z)k(\alpha\cdot z)t^{n-1}dtdz && (3.5)\\
&= \int_{\mathbb{R}^n} f(y+z)k(\alpha\cdot z)dz && (3.6)\\
&= \int_{\mathbb{R}} k(s)\int_{\alpha^\perp} f\Big((\alpha\cdot y+s)\alpha+z^\perp\Big)dz^\perp ds && (3.7)\\
&= \int_{\mathbb{R}} k(s)\hat{f}(\alpha, s+\alpha\cdot y)ds && (3.8)\\
&= \int_{\mathbb{R}} k(p-y\cdot\alpha)\hat{f}(\alpha,p)ds. && (3.9)
\end{aligned}$$

■

Lemma 2 (Grangeat's Formula) *Let* $f \in \mathcal{C}_0^\infty(\mathbb{R}^3)$. *Then for every* $\theta \in S^2$,

$$\frac{\partial}{\partial p}\hat{f}(\alpha, p)|_{p=y\cdot\alpha} = \int_{S^2\cap\alpha^\perp} \nabla_\alpha g(y, \theta)d\theta, \tag{3.10}$$

where ∇_α *is the directional derivative acting on the second argument of* $g(y, \theta)$ *in the direction of* α.

The proof of Grangeat's formula relies on the previous Lemma 1.

PROOF: Recall Lemma 1, and let the distribution $k = \delta^{'}$, which is homogeneous of degree -2. Then

$$\begin{aligned}
\int_{\mathbb{R}} \hat{f}(\alpha, p)\delta^{'}(p - y \cdot \alpha) &= -\int_{\mathbb{R}} \frac{\partial}{\partial p}\hat{f}(\alpha, p)\delta(p - y \cdot \alpha)dp && (3.11)\\
&= -\frac{\partial}{\partial p}\hat{f}(\alpha, p)|_{p=y\cdot\alpha} && (3.12)\\
&= \int_{S^2} g(y, \theta)\delta^{'}(\alpha \cdot \theta)d\theta && (3.13)
\end{aligned}$$

Note that for every compactly supported distribution φ, and $\alpha \in S^2$,

$$\varphi^{'}(\alpha \cdot \theta) = \sum_i \alpha_i \frac{\partial}{\partial \theta_i}\varphi(\alpha \cdot \theta), \tag{3.14}$$

so with $\varphi = \delta$:

$$\begin{aligned}
\int_{S^2} g(y, \theta)\delta^{'}(\alpha \cdot \theta)d\theta &= -\int_{S^2} g(y, \theta)\sum_i \alpha_i \frac{\partial}{\partial \theta_i}\delta(\alpha \cdot \theta)d\theta\\
&= -\int_{S^2} \sum_i \alpha_i \frac{\partial}{\partial \theta_i} g(y, \theta)\delta(\alpha \cdot \theta)d\theta\\
&= -\int_{S^2} \nabla_\alpha g(y, \theta)\delta(\alpha \cdot \theta)d\theta\\
&= -\int_{S^2 \cap \alpha^\perp} \nabla_\alpha g(y, \theta)d\theta. && (3.15)
\end{aligned}$$

Therefore, this proves Grangeat's formula [11]. ■

CHAPTER FOUR: GENERAL SCHEME FOR CONSTRUCTING INVERSION ALGORITHMS FOR CONE BEAM CT

In this chapter, an overview of the general scheme for constructing inversion algorithms for cone beam CT is given.

4.1 General Definitions

Definition 1 *Let Γ be a finite union of smooth curves in $\mathbb{R}^3$:*

$$I := \bigcup [a_l, b_l] \to \mathbb{R}^3, I \in s \to y(s) \in \mathbb{R}^3, |\dot{y}(s)| \neq 0 \text{ on } I \tag{4.1}$$

where

$$-\infty < a_l < b_l < \infty, \dot{y}(s) := dy/ds$$

$$\beta(s,x) := \frac{x - y(s)}{|x - y(s)|}, x \in \mathbb{R}^3 \setminus \Gamma, s \in I;$$

$$\Pi(x,\xi) := \{z \in \mathbb{R}^3 : (z - x) \cdot \xi = 0\}.$$

$D_f(y,\beta)$ is the cone beam transform of f, and $\beta(s,x)$ is the unit vector directed from the source towards the reconstruction point x.

In what follows, f is assumed to be smooth and compactly supported. Additionally, f is identically zero in a neighborhood of the trajectory.

Definition 2 *Let $x \in \mathbb{R}^3$ and $\xi \in \mathbb{R}^3 - \{0\}$. The intersection points of $\Pi(x,\xi)$ with Γ are denoted $y(s_j)$ where $s_j = s_j(\xi, \xi \cdot x), j = 1, 2, ...$*

For $\beta \in S^2$, $\beta^\perp$ denotes the circle $\{\ \alpha \in S^2 : \alpha \cdot \beta = 0\ \}$ consisting of unit vectors perpendicular to β. Let $Crit(s,x)$ be the set of all directions α is in $\beta^\perp(s,x)$ such that the plane $\Pi(x,\alpha)$ is tangent to Γ or contains an endpoint of Γ. Denote by I_{reg} the set of all parameters s in I, for which the set $Crit(s,x)$ is included (but not equal) in $\beta^\perp(s,x)$. Finally, define $Crit(x)$ to be the union over all s in I of all $Crit(s,x)$. We can concisely reformulate the definitions as:

$$\begin{aligned} Crit(s,x) &:= \Big\{\alpha \in \beta^\perp(s,x) : \Pi(x,\alpha) \text{ is tangent to } \Gamma \\ &\qquad \textit{or } \Pi(x,\alpha) \text{ contains an endpoint of } \Gamma\Big\}, \\ I_{reg} &:= \Big\{s \in I : Crit(s,x) \subsetneq \beta^\perp(s,x)\Big\}, \\ Crit(x) &:= \bigcup_{s \in I} Crit(s,x). \end{aligned} \tag{4.2}$$

4.2 Conditions on the trajectory

For any given x in $\mathbb{R}^3$, where the function f needs to be computed, the trajectory Γ must satisfy the following main assumptions:

Property 1 (Tuy's Completeness Condition.) *Any plane through x intersects Γ at least at one point.*

Property 2 *For any $s \in I_{reg}(x)$, the number of directions in $Crit(s,x)$ is finite.*

Property 3 *For any $\alpha \in S^2 \setminus Crit(x)$, the number of points in $\Pi(x,\alpha) \cap \Gamma$ is finite.*

Additionally, consider a weight function $n(s,x,\alpha), s \in I_{reg}(x), \alpha \in \beta^{\perp}(s,x) \setminus Crit(s,x)$. The main assumptions on the function n are the following:

Property 4 *For almost all $\alpha \in S^2$,*

$$\sum_{j:y(s_j)\in C\cap\Pi(x,\alpha)} n(s_j,x,\alpha) = 1. \tag{4.3}$$

Property 5 *$n(s,x,\alpha)$ is a piecewise constant function.*

4.3 Katsevich's General Inversion Formula

Theorem 3 *For $x \in \mathbb{R}^3$,*

$$f(x) = -\frac{1}{4\pi^2}\int_I \sum_m \frac{c_m(s,x)}{|x-y(s)|}\int_0^{2\pi}\frac{\partial}{\partial q}D_f(y(q),\cos\gamma\beta(s,x))+\sin\gamma\alpha^{\perp}(s,x,\theta_m))|_{q=s}\frac{d\gamma}{\sin\gamma}ds, \tag{4.4}$$

θ is a polar angle in the plane perpendicular to $\beta(s,x)$.

$\alpha^{\perp}(s,x,\theta) := \alpha^{'}(\theta) = \beta(s,x)\times\alpha(\theta)$.

$\theta_m \in [0,\pi)$ are the points where the $\phi(s,x,\theta)$ is discontinuous, and $c_m(s,x)$ are values of the jumps:

$$c_m := \lim_{\epsilon\to 0^+}(\phi(s,x,\theta_m+\epsilon)-\phi(s,x,\theta_m-\epsilon)). \tag{4.5}$$

where the function ϕ is defined as follows:

$$\phi(s,x,\theta) := \mathrm{sgn}(\alpha\cdot\dot{y}(s))n(s,x,\alpha), \alpha = \alpha(\theta) \in \beta^{\perp}(s,x), \tag{4.6}$$

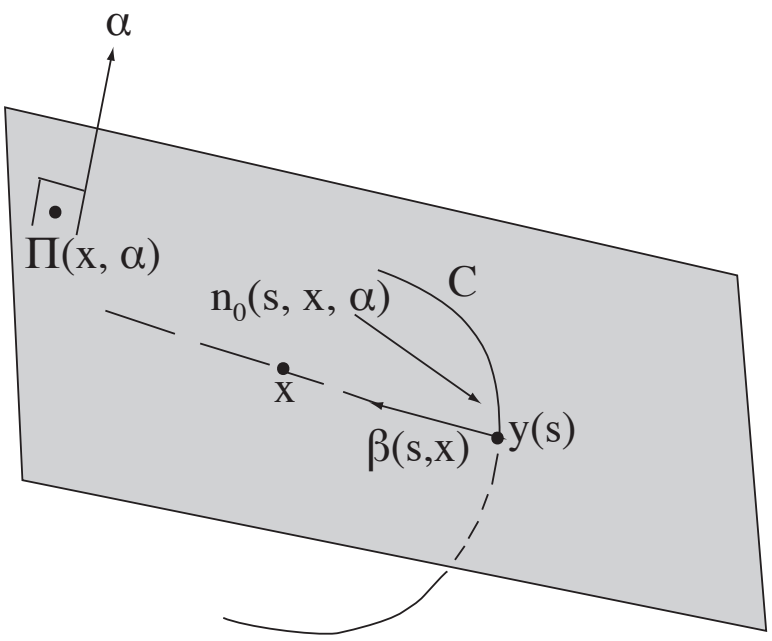

Figure 4.1: Illustration of the Weight Function

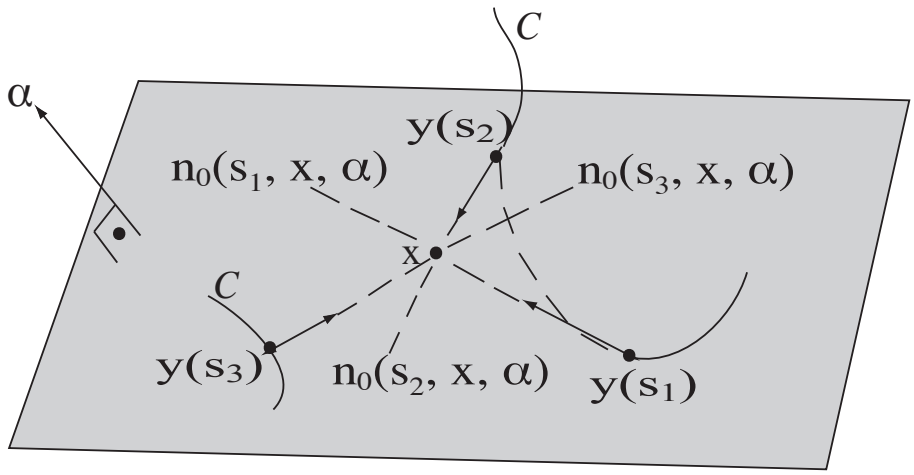

Figure 4.2: Illustration of the Normalization Condition

PROOF: This result is proven in [2]. However, let us give the main points of the proof. First define the following expression, which is similar to the 3-D Radon inversion formula, see Equation (2.19).

$$\begin{aligned}\mathcal{B}_\eta(f)(x) &:= -\frac{1}{8\pi^3}\int_{S^2}\sum_j \frac{n(s_j,x,\alpha)}{\alpha\cdot\dot{y}(s)} \\ &\times \frac{\partial}{\partial s}\Big\{\int_{\alpha^\perp}\nabla_{\Theta,\alpha}D_f(y(s),\Theta)d\Theta\Big\}|_{s=s_j}\eta(\alpha)d\alpha \end{aligned} \tag{4.7}$$

where $\nabla_{\Theta,\alpha}D_f(y(s),\theta)$ is the derivative of D_f with respect to Θ along the direction α. Explicitly,

$$\nabla_{\Theta,\alpha}D_f(y(s),\Theta) = \frac{\partial}{\partial t}D_f(y(s),\sqrt{1-t^2}\Theta + t\alpha)|_{t=0}, \Theta\in\alpha^\perp \tag{4.8}$$

Consider the following expression,

$$\frac{1}{\alpha\cdot\dot{y}(s_j)}\frac{\partial}{\partial s}\Big\{\int_{\alpha^\perp}\nabla_{\Theta,\alpha}D_f(y(s),\Theta)d\Theta\Big\}|_{s=s_j}. \tag{4.9}$$

Let us perform a change of variables by letting $p=\alpha\cdot\dot{y}(s)$. Then

$$\frac{\partial s}{\partial p} = \frac{1}{\alpha\cdot\dot{y}(s)} \tag{4.10}$$

Also, note that by Grangeat's formula, we have the following

$$\int_{\alpha^\perp}\nabla_{\Theta,\alpha}D_f(y(s),\Theta)d\Theta = \frac{\partial}{\partial p}\hat{f}(\alpha,p)|_{p=\alpha\cdot x}, \tag{4.11}$$

so

$$\frac{1}{\alpha\cdot\dot{y}(s_j)}\frac{\partial}{\partial s}\Big\{\int_{\alpha^\perp}\nabla_{\Theta,\alpha}D_f(y(s),\Theta)d\Theta\Big\}|_{s=s_j} = \frac{\partial^2}{\partial p}\hat{f}(\alpha,p)|_{p=\alpha\cdot y(s_j)=\alpha\cdot x} \tag{4.12}$$

Thus

$$\begin{aligned}\mathcal{B}_\eta(f)(x) &:= -\frac{1}{8\pi^3}\int_{S^2}\sum_j n(s_j,x,\alpha)\hat{f}_{pp}(\alpha,\alpha\cdot x)\eta(\alpha)d\alpha &(4.13)\\ &= -\frac{1}{8\pi^3}\int_{S^2}\hat{f}_{pp}(\alpha,\alpha\cdot x)\eta(\alpha)d\alpha &(4.14)\\ &= \frac{1}{8\pi^3}\int_{\mathbb{R}^3}\tilde{f}(\xi)\exp(-ix\cdot\xi)\eta\Big(\frac{\xi}{|\xi|}\Big)d\xi &(4.15)\end{aligned}$$

In the previous equations, we have used the fact that $\sum_j n(s_j) = 1$, and the Fourier Slice Theorem.

Another formula for $\mathcal{B}_\eta f(x)$ is derived in [2] and it is given by

$$\begin{aligned}(\mathcal{B}_\eta f)(x) = \frac{-1}{8\pi^2}\int_I \frac{1}{|x-y(s)|} &\times \int_0^{2\pi}\frac{\partial}{\partial\theta}\{\eta(\alpha)\mathrm{sgn}(\alpha\cdot\dot{y}(s))n(s,x,\alpha)\}\\ &\times \int_0^{2\pi}\frac{\partial}{\partial q}D_f(y(q),\cos\gamma\beta(s,x))\\ &+ \sin\gamma\alpha^\perp(s,x,\theta)|_{q=s}\frac{d\gamma}{\sin\gamma}d\theta ds &(4.16)\end{aligned}$$

where

$$\alpha(s,\theta)\in\beta^\perp(s,x),\ \alpha^\perp(s,x,\theta) := \beta(s,x)\times\alpha(s,\theta). \tag{4.17}$$

Denote

$$\phi(s,x,\theta) := \mathrm{sgn}(\alpha\cdot\dot{y}(s))n(s,x,\alpha), \alpha = \alpha(s,\theta)\in\beta^\perp(s,x) \tag{4.18}$$

As seen in the definition, the function ϕ depends on the signum function and on the weight function, which is piecewise constant. Thus ϕ is piecewise constant with discontinuities at θ_m, and the values of the jumps are denoted by c_m. As a result, $\frac{\partial}{\partial\theta}$ in the formula for $\mathcal{B}_\eta f$ will yield delta functions, and thus the integral with respect to θ becomes a summation over all jumps c_m. It is important to observe that, due to properties 2 and 3, the number of terms

in the summation involved in Katsevich's formula is finite. Katsevich's inversion formula is obtained by letting $\eta \to 1$ and by using the Fourier inversion formula. ■

As a final remark, it is important to mention that for $\alpha \in \beta^{\perp}(s,x)$, the planes $\Pi\Big(y(s), \alpha(s,\theta_m)\Big)$ form the set of filtering planes for any given point (s,x). For a fixed m, since $\beta \perp \alpha$, then the integral with respect to γ in Katsevich's Formula is confined to the corresponding filtering plane. In practice, the intersections of such planes with the detector is referred to as filtering lines.

CHAPTER FIVE: THE CIRCLE AND LINE ALGORITHM

5.1 Introduction and General Settings

In practice, there are many different medical imaging devices that can collect x-ray scans. In this research, the C-arm is the medical device that is being considered. In order to collect x-ray scans, the operator first moves the patient along a line and subsequently rotates the C-arm around the patient. Such a movement generates a trajectory composed of a incomplete circle and a line (C-L trajectory), for which an inversion formula was developed in 2004 by Katsevich. Note that the inversion formula for the C-L trajectory is a special case of the general scheme previously studied in Chapter 4. Below are discussed the general settings of the C-L problem.

The trajectory consists of an incomplete circle C and a line segment L attached to C. It is assumed that C is sufficiently close to a complete circle and that L is sufficiently long. Let y_0 be the point where the circle and the line intersect. Let the following be respective parametrizations of the line and circle, $s \in I_1 : s \to y(s) \in L$ and $s \in I_2 : s \to y(s) \in C$.

Given a circle of radius R, assume U is an open set contained in the cylinder $\{(x_1, x_2, x_3) \in \mathbb{R}^3 : x_1^2 + x_2^2 < R\}$. Let x be a reconstruction point in U. Consider the plane $\Pi(x)$ through x and L. $\Pi(x)$ intersects the circle C at two points, one of them is y_0, and the other is $y_C(x)$. Let the line segment containing x and joining the point $y_C(x)$ to L be denoted by $L_{1\pi}$. Then $y_L(x)$ denotes the other endpoint of $L_{1\pi}(x)$

There are two parametric intervals. The first one is $I_1(x) \subset I_1$ which corresponds to the

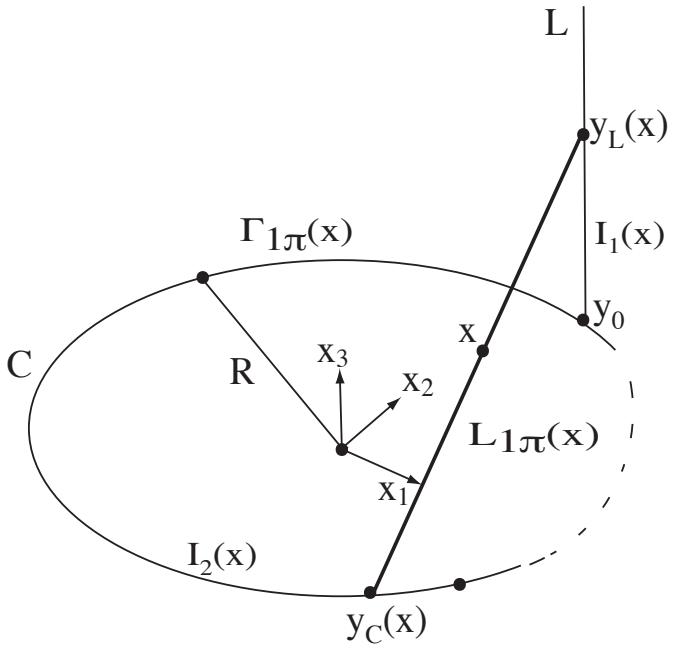

Figure 5.1: Circle and Line Trajectory

section of L between y_0 and $y_L(x)$. The second interval $I_2(x)$ corresponds to the section of the circle between y_0 and $y_C(x)$. $\Gamma_{1\pi}(x)$ denotes the section of $C \bigcup L$ bounded by $L_{1\pi}(x)$.

In order to utilize the result of the general scheme, we must show that for every point x in the region of interest, the curve $\Gamma_{1\pi}(x)$ satisfies the conditions of the general inversion formula.

Since $\Gamma_{1\pi}(x)$ is determined via the line $L_{1\pi}$, then is is clear that any plane through x intersects $\Gamma_{1\pi}$ at least once. Therefore Tuy's completeness property is satisfied.

Consider $y(s) \in \Gamma_{1\pi}(x)$ such that $y(s) \notin \{y_0, y_C(x), y_L(x)\}$. First assume that the source $y(s) \in C$. Thus if $\Pi(x)$ is tangent to C, and contains either the line $L_{1\pi}$, or the point y_0, then the vector $\alpha \in Crit(s,x)$. There are at most three such planes. Second, assume that the source $y(s) \in L$. Then the vector $\alpha \in Crit(s,x)$ if $\Pi(x)$ is tangent to $C \cap \Gamma_{1\pi}(x)$ or contains L. In this case, $\Pi(x)$ also contains the line $L_{1\pi}$. There are only two such planes. Therefore, Property 2 is satisfied.

To show that Property 3 is satisfied, consider the intersection of planes through x with $\Gamma_{1\pi}(x)$. Planes tangents to the trajectory are neglected. The number of intersection points (IPs) is either one or three. Thus Property 3 is satisfied. In addition, there can be only one IP on the line L.

The weight function $n(s,x,\alpha)$ satisfies Properties 4, and 5. Indeed, if there is only one IP, then it is given weight 1. If there are three IPs, then the two IPs on the circle have weight 1, and the IP on the line has weight -1.

5.2 Katsevich's Inversion Formula for the Circle and Line Trajectory

Theorem 4 *For $f \in C_0^\infty(U)$,*

$$f(x) = -\frac{1}{2\pi^2} \int_{I_k(x)} \sum_{k=1}^{2} \frac{\delta_k(s,x)}{|x - y(s)|} \int_0^{2\pi} \frac{\partial}{\partial q} g(y(q), \Theta_k(s,x,\gamma))|_{q=s} \frac{d\gamma}{\sin\gamma} ds, \tag{5.1}$$

where

$$\Theta_k(s,x,\gamma) := \cos\gamma\beta(s,x) + \sin\gamma e_k(s,x), \;\; e_k(s,x) := \beta(s,x) \times u_k(s,x), \tag{5.2}$$

and δ_k is defined as follows:

$$\delta_1(s,x) = -\mathrm{sgn}(u_1(s,x) \cdot \dot{y}(s)), \;\; s \in I_1(x); \;\; \delta_2(s,x) = 1, \;\; s \in I_2(x). \tag{5.3}$$

Proof: A complete proof can be found in [2]. Below is a sketch of the proof. Consider $\phi(s,x,\theta)$ defined in (4.6). The purpose is to locate the jumps of the function ϕ. First let us assume that the source is on the line. By projecting the curve onto the detector denoted by $DP(s)$, we obtain a parabola whose equation is

$$w = -\frac{h}{2}\Big(\frac{u^2}{R^2} + 1\Big). \tag{5.4}$$

It is important to mention that the detector plane $DP(s)$ contains the x_3–axis and is perpendicular to the shortest line segment connecting the source position $y(s)$ and the x_3–axis. The center of $DP(s)$ is chosen to be at $(0,0,h)$. Finally, the first axis of $DP(s)$ is horizontal and the second axis is vertical. See Figure 5.2 for illustration.

Refer to figure 5.3 for the following discussion. We find θ_1 such that $\Pi(s,\theta_1)$ contains the reconstruction point x and the line L. In orther words, $\dot{y}(s) \perp \alpha(\theta_1)$. Since $\alpha_- \cdot \dot{y}(s) < 0$ and $\alpha_+ \cdot \dot{y}(s) > 0$, then we respectively have $\mathrm{sgn}(\alpha(\theta_-) \cdot \dot{y}(s)) = -1$ and $\mathrm{sgn}(\alpha(\theta_+) \cdot \dot{y}(s)) = 1$.

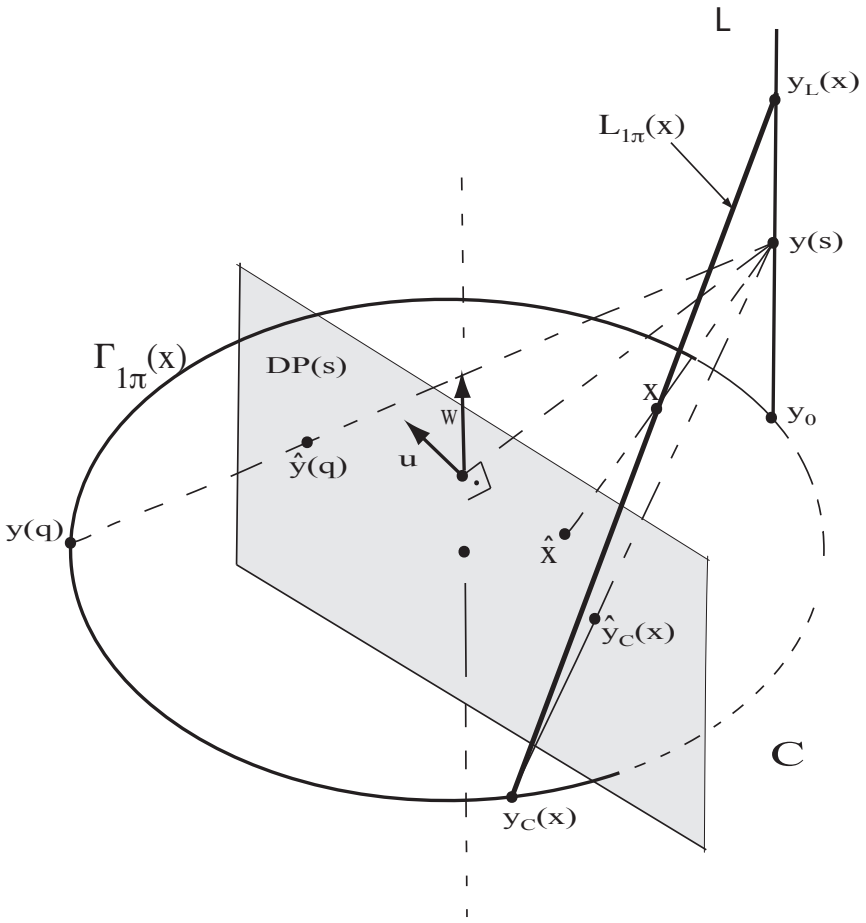

Figure 5.2: Projection when the source is located on the line

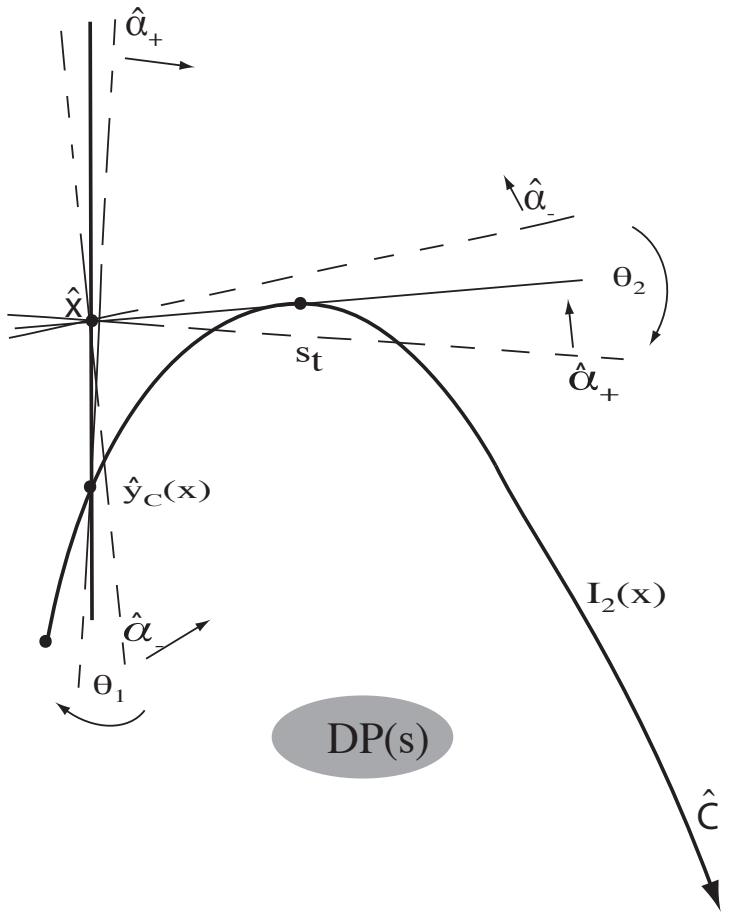

Figure 5.3: Projection when the source is located on the line

The number of IPs of $\Pi(s, x, \theta)$ with the C-L trajectory changes from 3 to 1 between α_- and α_+. Consequently,

$$n(s, x, \alpha_-) = -1, n(s, x, \alpha_+) = 1. \tag{5.5}$$

It is also important to mention that the signum function jumps from -1 to 1. Consequently, the function ϕ is continuous across $\theta = \theta_1$. Indeed, depending on the direction of $\dot{y}(s)$, we either have

$$\phi(s, x, \theta_-) = \phi(s, x, \theta_+) = 1. \tag{5.6}$$

or

$$\phi(s, x, \theta_-) = \phi(s, x, \theta_+) = -1. \tag{5.7}$$

Therefore, the function ϕ is continuous regardless of the direction of $\dot{y}(s)$.

Now let us find θ_2 s.t $\Pi(s, \theta_2)$ is tangent to C at some $y(s_t)$ where $s_t \in I_2$. The number of IPs varies from 1 to 3 with a jump from $n(s, x, \alpha_-) = 1$ to $n(s, x, \alpha_+) = -1$ on the line. Therefore,

$$[\phi(s, x, \theta)]_{\theta=\theta_2} = -2 \text{ sgn}(\alpha \cdot \dot{y}(s)), \tag{5.8}$$

where -2 is the value of the jump.

Next, we assume that the source is on the circle as illustrated in Figure 5.4.

We find θ_1 s.t $\Pi(s, \theta_1)$ contains y_0, θ_2 s.t $\Pi(s, \theta_2)$ contains $L_{1\pi}$, and θ_3 s.t $\Pi(s, \theta_3)$ is tangent to C at some point $y(s_t)$, where $s_t \in I_2$. In these conditions, $n(s, x, \theta) = 1$, for all θ. Thus, only the signum function will create jumps. As a fact, $\text{sgn}(s, x, \alpha_-) = -1$ and

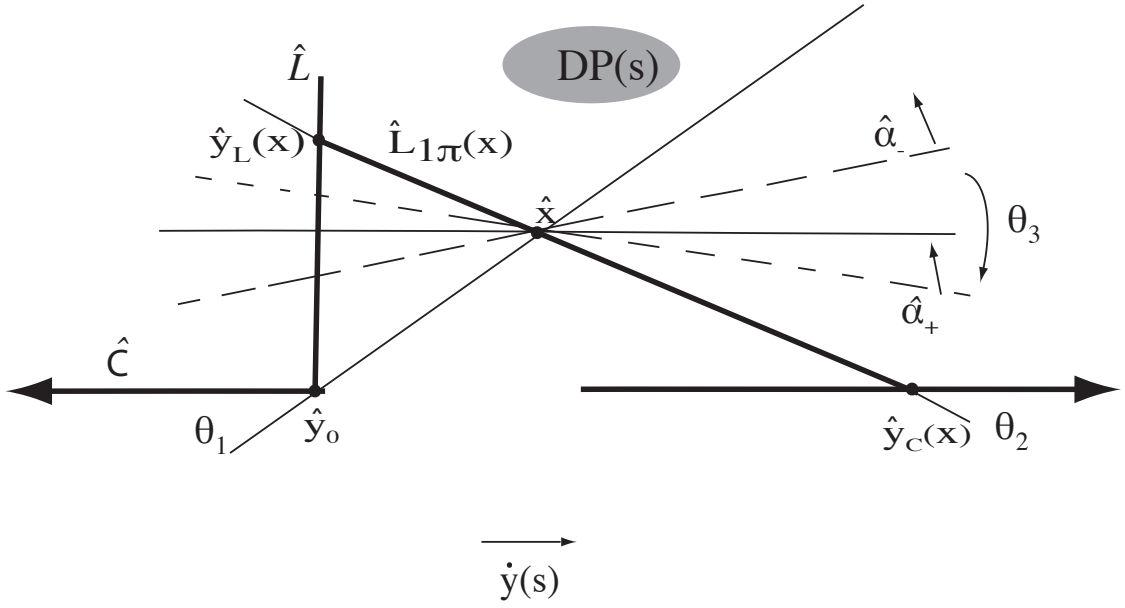

Figure 5.4: Projection when the source is located on the circle

$\mathrm{sgn}(s, x, \alpha_+) = 1$. This indicates a jump whose value is 2. Thus, we have the following

$$[\phi(s, x, \theta)]_{\theta=\theta_3} = 2, \ s \in I_2. \tag{5.9}$$

Also note that by construction $\mathrm{sgn}(\alpha(\theta) \cdot \dot{y}(s))$ is continuous across θ_1 and θ_2.

By using the above results, an inversion formula for the C-L can be formulated. Given a point $y(s)$ on the line, find the plane P_1 passing through x and $y(s)$, and tangent to C at some point $y(s_t)$. Define the vector

$$u_1(s, x) := \frac{(y(s_t) - y(s)) \times \beta(s, x)}{|(y(s_t) - y(s)) \times \beta(s, x)|}, \ x \in U, \ s \in I_1(x). \tag{5.10}$$

Pick a point $y(s)$ on the circle, and let P_2 be the plane containing the point x and tangent to the trajectory at $y(s)$.

Define the vector

$$u_2(s, x) := \frac{\dot{y}(s) \times \beta(s, x)}{|\dot{y}(s) \times \beta(s, x)|}, \ x \in U, \ s \in I_2(x). \tag{5.11}$$

Note that the vector u_1 and u_2 are orthogonal to P_1 and P_2 respectively. Katsevich's reconstruction formula $(5.1) - (5.3)$ can thus be obtained from $(5.8) - (5.11)$.

■

CHAPTER SIX: THE DISTORTED CIRCLE AND LINE ALGORITHM

6.1 Motivation and Research Outline

As mentioned in the previous chapter, the circle and line source trajectory is obtained by moving the patient along a line and by rotating the C-arm, which is a common X-ray device that can collect cone beam data. In practice, due to the heavy weight of the C-arm, the presumed circular trajectory of the C-arm is frequently perturbed. It is important to mention that if the distortions on the source trajectory are not corrected, they lead to some noticeable artifacts in the reconstructed image.

An FBP-type (Filtered Backprojection) algorithm was developed for the ideal circle and line source trajectory by Katsevich in 2004. This means that two steps are involved in the numerical implementation of the algorithm. First, one performs a shift-invariant filtering of the derivative of the cone beam projections. Second, the result of the filtering is back-projected in order to reconstruct the image. In this algorithm, the number of intersection points between the planes and the source trajectory was established to be at most three. The main idea of this research is to utilize Katsevich 's algorithm as a building block for constructing an inversion algorithm for a broader class of curves.

The problem is solved in the following manner. The first step is to consider an entire class of curves on which a set of natural geometric restrictions is imposed. The curves are assumed to be planar, smooth, non self-intersecting with positive curvature. Also, the curves

have to satisfy an extra condition referred to as "convexity with respect to the origin". A given curve satisfies the "convexity with respect to the origin" if the number of intersection points between the curve and a line passing through its initial point is at most two.

The next step is to study the geometry of the intersection points (IPs) between planes and the source trajectory. The distribution of the IPs over different sections of the source trajectory is also taken into consideration in this analysis. The plan is to limit the number of IPs between planes and the source trajectory to maximum three as prescribed by Katsevich's ideal circle-and-line algorithm.

Third, a set of lemmas is derived proving that Katsevich's inversion formula for the ideal circle-and-line can be applied to our class of curves.

In summary, the derived results will apply not only to the ideal circle, but they will also be applicable to the entire class of curves defined earlier. In other words, any curve or source trajectory satisfying the prescribed conditions will admit an FBP-type reconstruction.

6.2 Class of Curves

Definition 3 *Let $y(s), s \in [0, s_{max}]$ be a planar curve. The curve C is said to be convex with respect to $y(0)$ its initial point, if any line passing through $y(0)$ intersects C at most twice.*

Definition 4 *$\mathscr{C}$ is defined as the class of non self-intersecting smooth planar curves with positive curvature satisfying the convexity with respect to $y(0)$.*

Lemma 3 *Let $C \in \mathscr{C}$, L_1 be a line in the plane. Assume that C intersects the line L_1 at some point s_1. Let $\vec{T}(s_1)$, $\vec{N}(s_1)$ be the unit tangent and the unit normal respectively as*

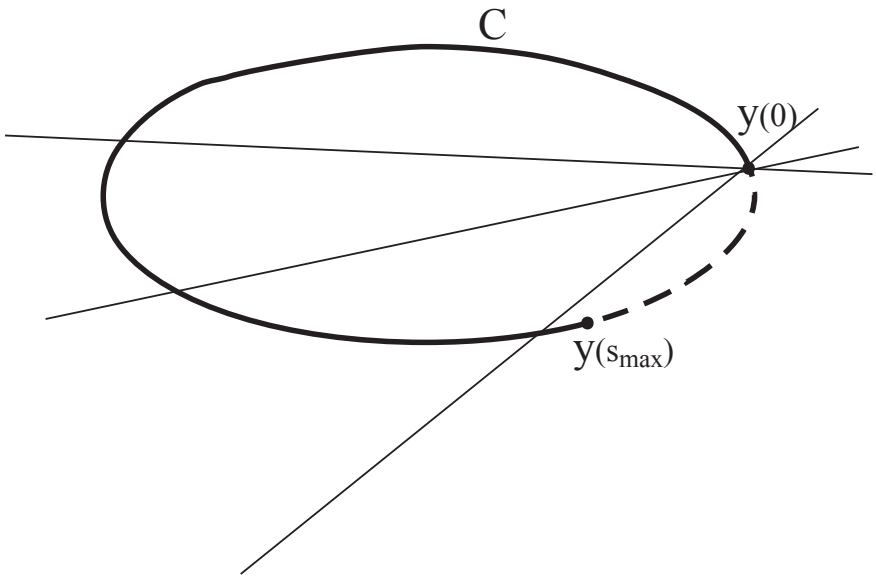

Figure 6.1: Illustration of the convexity with respect to y(0)

illustrated in Figure 6.2. Then the next closest intersection point s_2 with the curve C and the line L_1, if it exists, satisfies $\Big(y(s_2) - y(s_1)\Big) \cdot \vec{N}(s_1) > 0$.

PROOF: Let $C \in \mathscr{C}$, L_1 be a line in the plane. Let s_1 be the intersection point between the curve C and L_1 as depicted in Figure 6.2. Let us introduce the xy rectangular coordinate system where the x-axis is parallel to L_1 and the y-axis is perpendicular to L_1. See Figure 6.3 for an illustration. Let s be a point on C, and consider the initial condition depicted in Figure 6.3, then there exists a point at which the tangent line T_1 is horizontal.

First, if the vertical coordinate of the point s on the curve C strictly decreases, then the curve will eventually intersect the line L_1. Therefore, we are done in this case. See top left panel of Figure 6.3.

Second, let T_s be the tangent lines to C at s, and assume C crosses the tangent line T_1, which was previously defined. In this case, the tangent lines T_s change direction of rotation as illustrated in Figure 6.3. This means there is a point s^* at which the tangent T^* to C stops rotating. Equivalently, s^* is a point at which the curvature is zero. This is contradictory because by definition C has a positive curvature for all s. See bottom left panel of Figure 6.3.

Third, if C continues to curve, then there is another point at which the tangent T_2 is horizontal. The endpoint of the curve is contained in the region bounded by the curve, T_1, and T_2. By repeating the process, then the endpoint of the curve C is trapped in a spiral. Consequently, it is clear that the curve C will never intersect the line L_1. See bottom right panel of Figure 6.3.

■

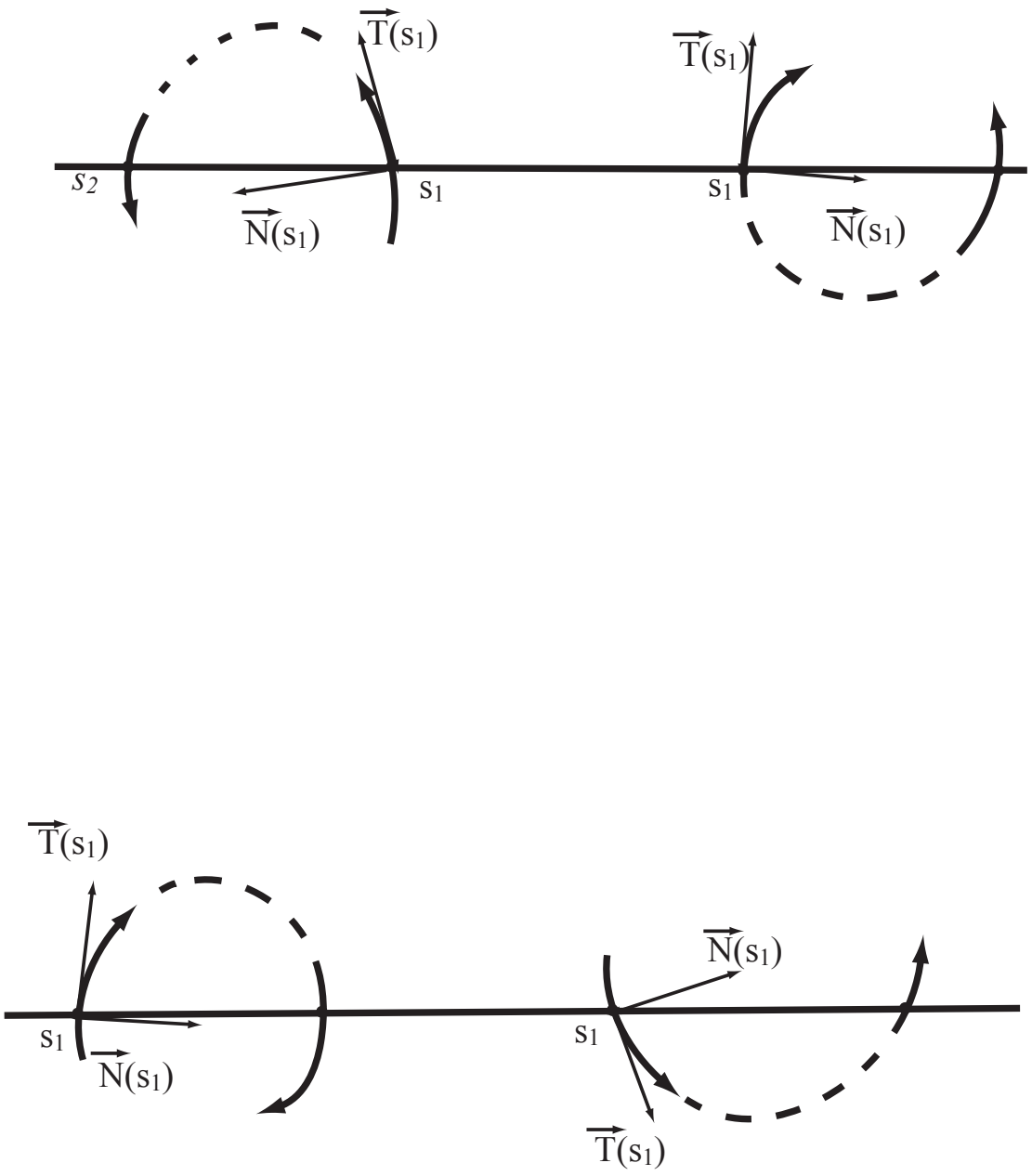

Figure 6.2: Illustration of Lemma 3

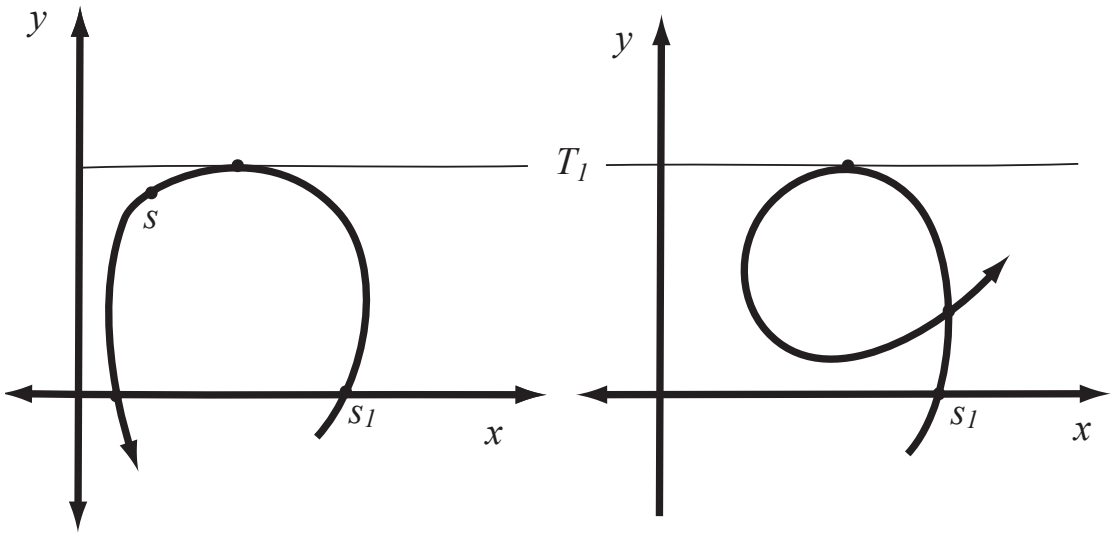

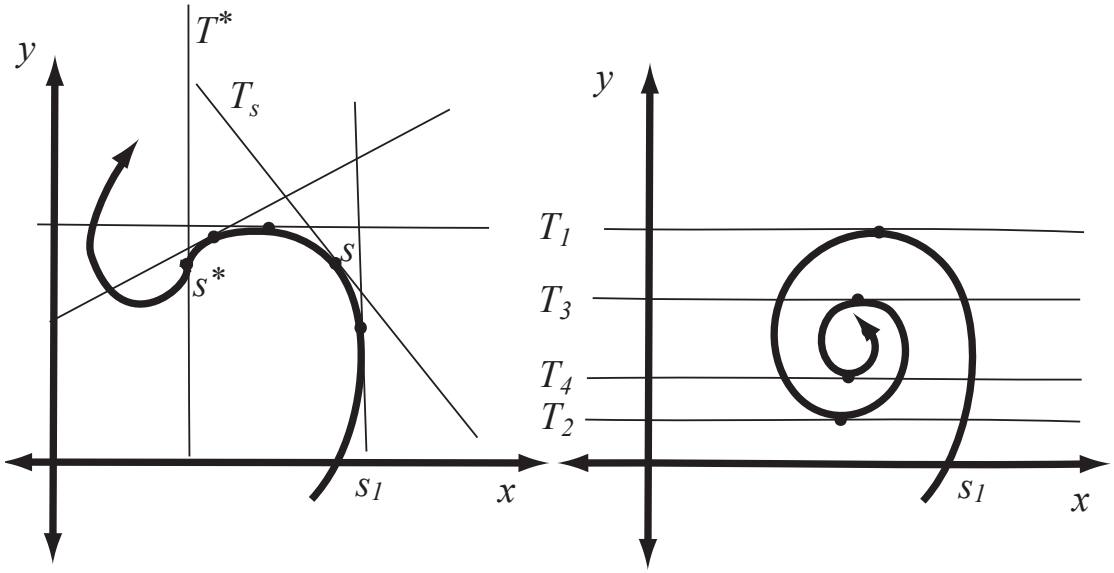

Figure 6.3: Illustration of the Proof of Lemma 3

Lemma 4 *Let $C \in \mathscr{C}$ and L_1 be a line in the plane. Then the number of intersection points with the curve C and the line L_1 does not exceed two.*

PROOF: For a contradiction, assume there are three intersection points s_1 , s_2 and s_3 with the curve C and the line L_1 as illustrated in Figure 6.4. Let $\vec{N}(s)$ and $\vec{T}(s)$ respectively the unit tangent and normal vectors at s. It is assumed that C starts at s_1, so by Lemma 3, the next intersection point s_2 satisfies $\Big(y(s_2) - y(s_1)\Big) \cdot \vec{N}(s_1) > 0$. Similarly by Lemma 3, the point s_3 satisfies $\Big(y(s_3) - y(s_2)\Big) \cdot \vec{N}(s_2) > 0$, and it is located either on the right of s_1 or on the left of s_1. Let s^* be a point in the plane.

First, if the point s_3 is located on the right of s_1, then there is a line passing through s^* and s_1 that intersects C at least once.

Second, if the point s_3 is between the points s_1 and s_2, then there is a line passing through s^* and s_3 that intersects C at least once. These statements hold true for the origin $s = 0$ in particular. In either case, the convexity with respect to the origin is violated. This ends the proof. ■

Lemma 5 *Let $C \in \mathscr{C}$. Consider $y(s_1)$ and $y(s_2)$ two distinct source positions such that $s_1 \neq s_2$. Then there is no line intersecting C at s_1 and tangent to the curve C at s_2.*

PROOF: Let $y(s_1)$ and $y(s_2)$ be two distinct source positions such that $s_1 < s_2$. For a contradiction, assume there is a line intersecting C at s_1 and tangent to the curve C at s_2 as depicted in Figure 6.5. Denote by T_1 the tangent line to C at the point s_2. Since the curvature is non zero, then the curve C is entirely on one side of the tangent line T_1. Consequently, the rotation of T_1 around s_1 will create two more intersection points between

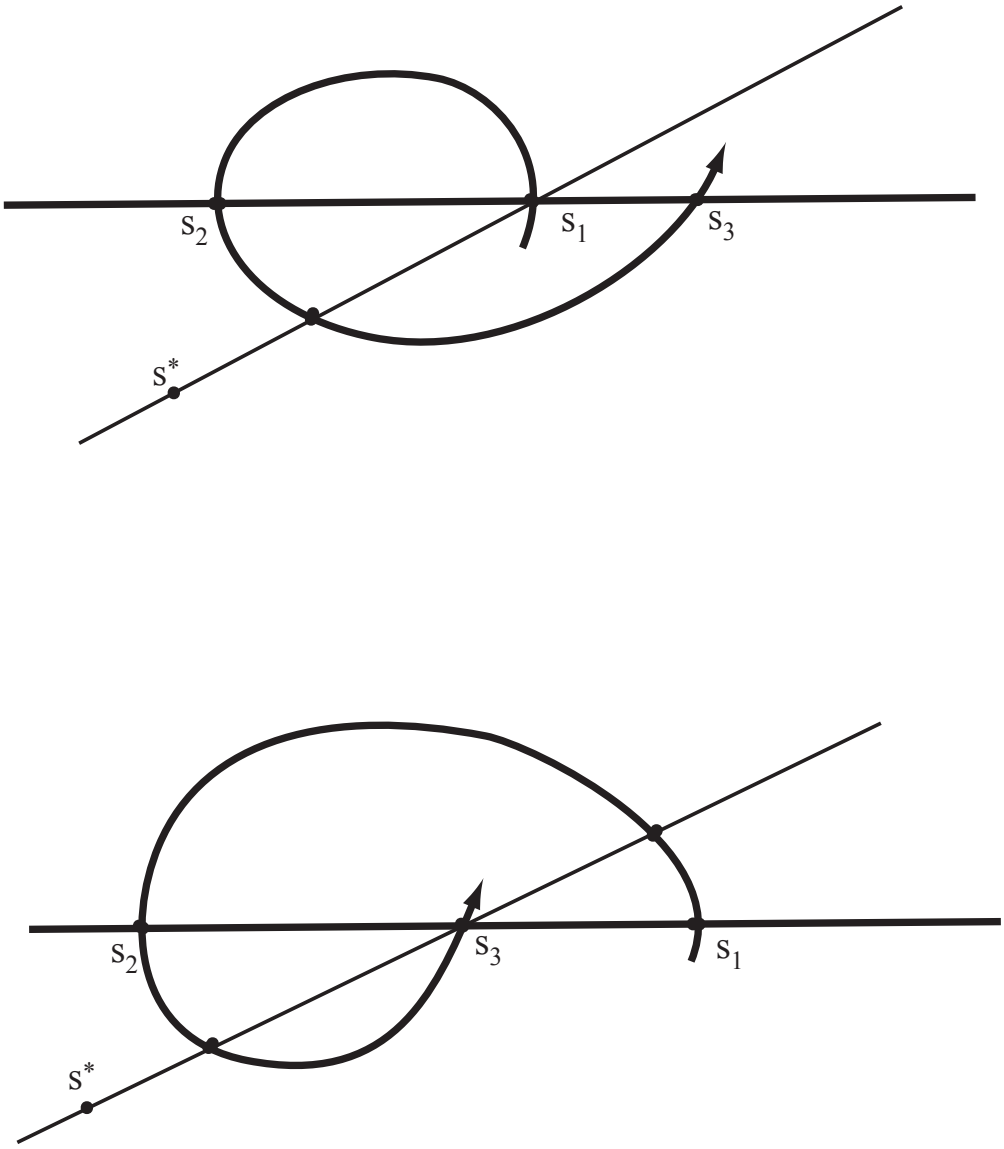

Figure 6.4: Illustration of the Proof of Lemma 4

T_1 and C. Lemma 4 is thus contradicted. ■

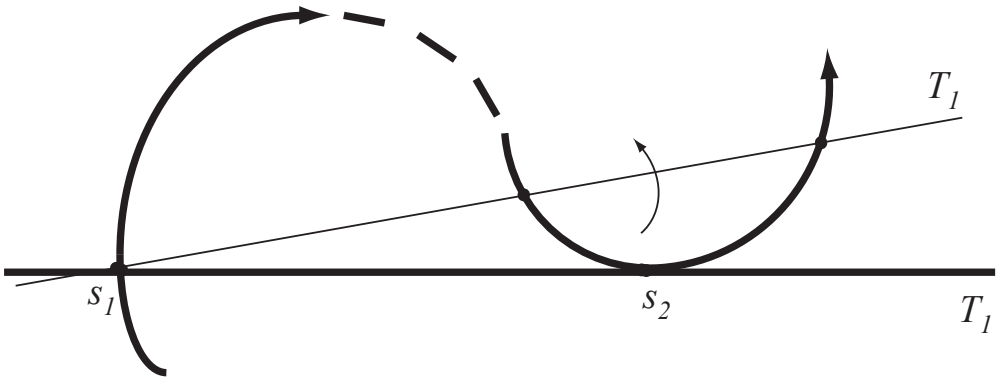

Figure 6.5: Illustration of Lemma 5

The lemmas derived so far will help us find a parametrization for the distorted circle.

6.3 The Distorted Circle

Given a curve $C \in \mathscr{C}$, we would like to find an appropriate parametrization for the distorted circle. This leads us to think about the parametrization below:

$$y(s) = \Big(R(s)\cos(s), R(s)\sin(s), 0\Big), s \in [0, s_{max}], \tag{6.1}$$

where $R(s)$ is a radius function.

However some questions arise with this representation. First, we need to establish the existence of $R(s)$ for all $s \in [0, s_{max}]$ by using Lemma 4. Second, we have to show that R is well-defined and is a smooth function of s. Note that the choice of the radius function R is not unique.

6.3.1 Existence and Smoothness of R(s)

Lemma 6 *Let $C \in \mathscr{C}$, $y(s) \in C, s \in [0, s_{max}]$. Then, there exists a well defined smooth function R such that $y(s) = (R(s)\cos(s), R(s)\sin(s), 0)$.*

PROOF: Let $s = 0$, s_{max} be respectively the initial and the terminal point of the curve C. Let $x^{'}y^{'}$ be the rectangular coordinate system originated at $s = 0$, and whose horizontal axis $x^{'}$ is tangent to the curve C at $s = 0$. While the horizontal axis points to the same direction as the tangent vector at $s = 0$, the vertical axis $y^{'}$ has the same direction as the normal vector to the curve C at the initial point $s = 0$ as depicted in Figure 6.6. Two cases need to be considered.

For the first case, we consider the positive portion of the $y^{'}$ axis. Assume C intersects the positive portion of the $y^{'}$ axis at s_t. By construction the point s_t is above the origin $s = 0$. Choose any point P located on the $y^{'}$ axis between $s = 0$ and s_t. The idea is to show that any ray with vertex at P intersects the curve C at most once. For this matter, define L_1 to be the line containing the ray with vertex at P. For the proof, we will only need to consider the intersections between C and the portion of L_1 where the ray is located. Since $s = 0$ and s_{max} are on different sides of L_1, there can be only an odd number of intersection points with the curve and the line L_1. Since by Lemma 4, we cannot have three intersection points, then there must be only one with the curve and the line L_1. See top panel of Figure 6.6.

For the second case, assume C does not intersect the positive portion of the $y^{'}$ axis. Let s be a point on the curve C, and let $l(s)$ be the tangent lines to C at s. For every s, the line $l(s)$ intersects the $y^{'}$ axis at some point $Q(s)$. Of all the points $Q(s)$, the one obtained when $s = s_{max}$, denoted Q_t is the lowest on the positive portion of the $y^{'}$ axis. Let P be a point located on the line segment between the origin $s = 0$ and the point Q_t. Also, if we assume that the ray with vertex at P intersects the curve C at s_1 and s_2, then we can find a point s^* on C such that $s^* \neq s_1, s_2$, as shown in Figure 6.6. Additionally, denote by L_1 the line containing the ray with vertex at P. Then the tangent line $l(s^*)$ to C at s^* intersects the positive portion of the $y^{'}$ axis at Q^*, which is a point located below Q_t on the $y^{'}$ axis. See bottom panel of Figure 6.6. The statement is a contradiction because by construction, the point Q_t is the lowest point located on the positive portion of the $y^{'}$ axis. The existence of the function R is thus established. See bottom panel of Figure 6.6.

Since the radius function R is well defined for all s in $[0, s_{max}]$, we now need to prove that R is also a smooth function of s. For the proof, consider the rectangular coordinate system originated at the center of the distorted circle i.e the point P previously defined in the proof. The x-axis is the horizontal axis while the y-axis is the vertical axis as depicted in Figure 6.7.

Let $\vec{Y}(t) = \Big(x(t), y(t)\Big)$ be a parametrization of a point on the distorted circle. We have the following

$$x(t) = R(t)\cos(s) \tag{6.2}$$

$$y(t) = R(t)\sin(s) \tag{6.3}$$

The above system can be rewritten in a compact form

$$R(t)\vec{\Theta}(s) - \vec{Y}(t) = 0, \tag{6.4}$$

where $\vec{\Theta}(s) = (\cos(s), \sin(s))$ and $\vec{Y}(t) = (x(t), y(t))$. Since $\vec{Y}(t)$ is smooth, then $R(t) = \sqrt{x^2(t) + y^2(t)}$ must be smooth. Consequently we can differentiate Equation 6.4 with respect to the variable t. We then obtain

$$\dot{R}(t)\vec{\Theta}(s) + R(t)\dot{\vec{\Theta}}_s\frac{ds}{dt} - \dot{\vec{Y}}(t) = 0 \tag{6.5}$$

By applying the dot product to Equation 6.5 with the vector $\vec{\Theta}^{\perp}$, and using the equality $\vec{\Theta}^{\perp} = \dot{\vec{\Theta}}_s$, we obtain the expression below

$$R(t)\frac{ds}{dt} - \dot{\vec{Y}}(t)\cdot\Theta^{\perp} = 0 \tag{6.6}$$

since $\vec{\Theta}\cdot\vec{\Theta}^{\perp} = 0$ and $\dot{\vec{\Theta}}_s\cdot\vec{\Theta}^{\perp} = 1$. In the above equation, R is a positive function of t, and the expression $\dot{\vec{Y}}\cdot\Theta^{\perp}$ is non zero. For a contradiction, if we assume $\dot{\vec{Y}}\cdot\Theta^{\perp} = 0$, then this

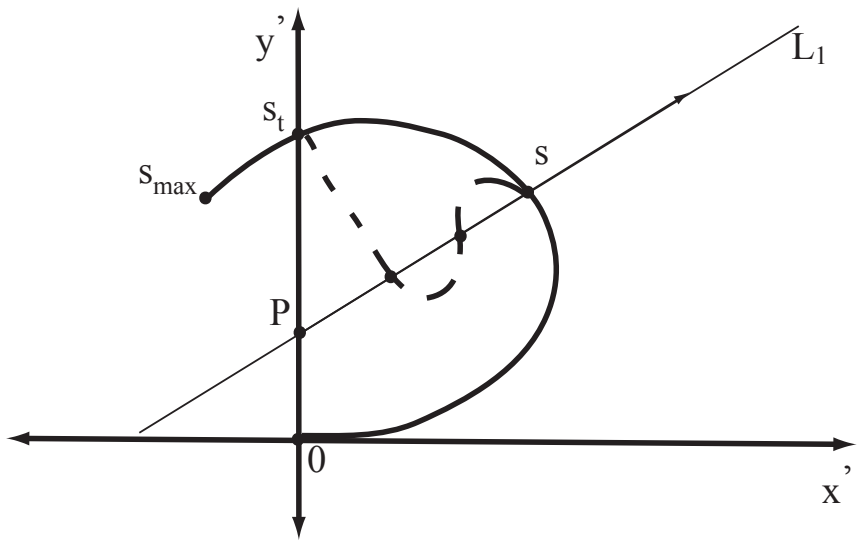

Case 1: The curve C intersects the vertical axis

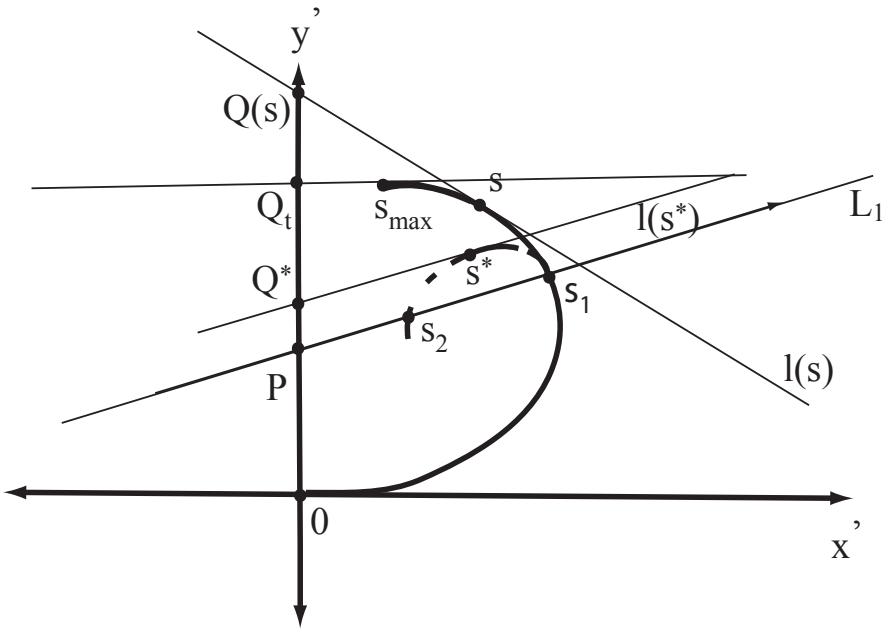

Contradiction when the ray intersects C twice

Figure 6.6: Existence of the Function $R(s)$

is equivalent to saying that the vector $\vec{\dot{Y}}$ is parallel to $\vec{\Theta}$, which is impossible according to Lemma 5. See bottom panel of Figure 6.7 for an illustration.

The fact that $\vec{\dot{Y}} \cdot \Theta^{\perp}$ is non zero implies that $\frac{ds}{dt}$ is also non zero. Therefore, we can write t as a function of s i.e $t = t(s)$, and the function $t = t(s)$ is continuously differentiable by the Implicit Function Theorem. Consequently, the radius function $R(t) = R(t(s))$ is a smooth function of s.

■

6.3.2 Choice of R(s) and its Consequence

We have shown that R exists and is a smooth function of s. However, the choice of $R(s)$ is not unique. In our case, we choose the function R in the following manner. Recall the cartesian coordinate system $x - y$ introduced earlier in the proof of Lemma 6. See Figure 6.8 for an illustration. With such a choice for $R(s)$, we have the lemma below.

Lemma 7 *$R(0) - R(s)\cos(s) > 0$ for all s in $[0, s_{max}]$.*

PROOF: In what follows, see the illustration in Figure 6.8. Let $x(s) = R(s)\cos(s)$ be the horizontal coordinate of a point s on the curve C. If $s = 0$, then $x(s) = x(0) = R(0)$. Since C has a positive curvature, then $x(s) < x(0)$. In other words, $R(0) - R(s)\cos(s) > 0$. ■

6.3.3 The Pi Line and its Properties

The source trajectory consists of a distorted circle C and a line L attached to C at some point $y(0)$. The curve C is relatively close to a complete circle and the line L is sufficiently long. Let the following be respective parametrizations of the line and circle, $s \in I_1 : s \rightarrow y(s) \in L$

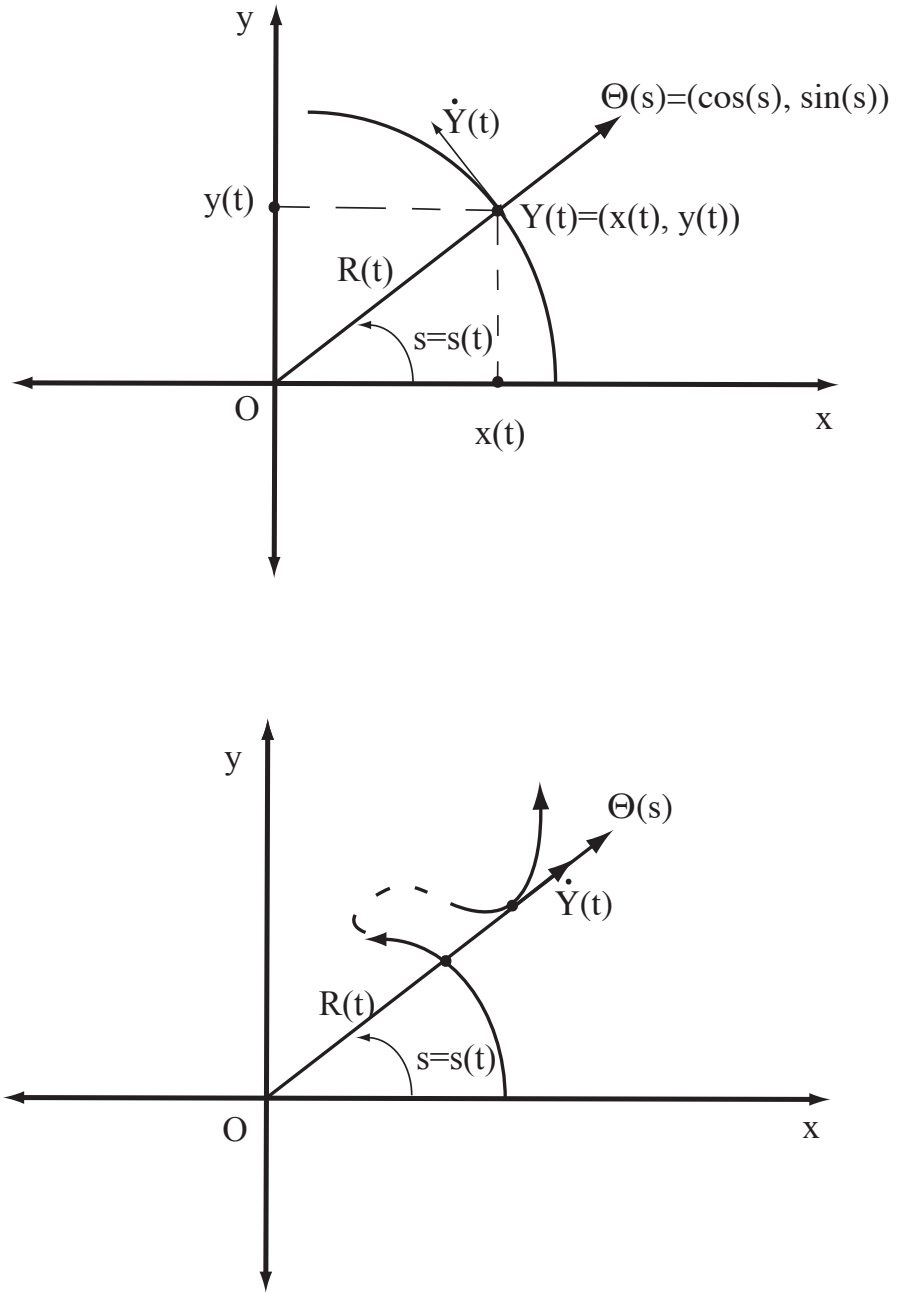

Contradiction when Θ is parallel to $\dot{Y}$

Figure 6.7: Existence and Smoothness of $R(s)$

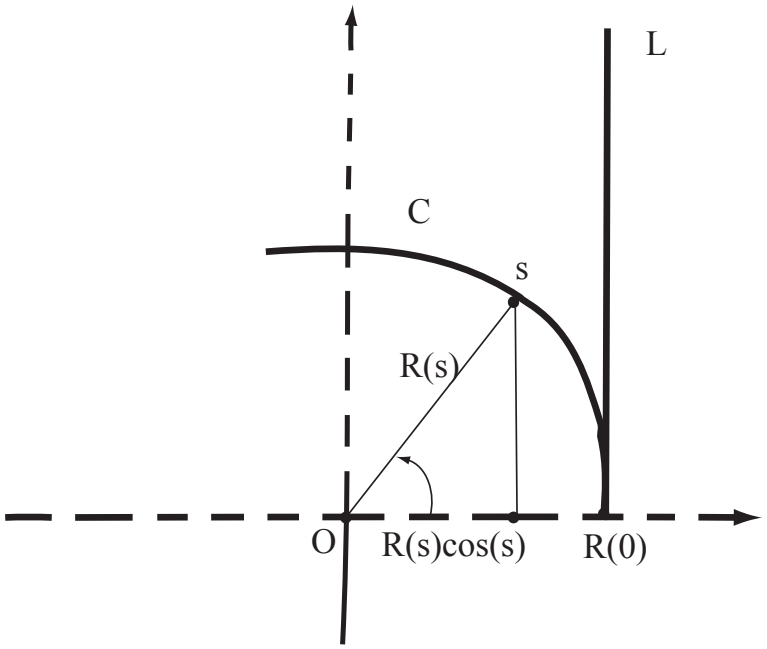

Figure 6.8: $R(0) - R(s)\cos(s) > 0$

and $s \in I_2 : s \to y(s) \in C$. In what follows, we recall the general settings of the ideal circle and line source trajectory introduced in Chapter 5, and we use Figure 5.1 as an illustration.

Consider the following two parametric intervals. The first one is $I_1(x) \subset I_1$ which corresponds to the section of L between $y(0)$ and $y_L(x)$. The second interval $I_2(x)$ corresponds to the section of the circle between $y(0)$ and $y_C(x)$. $\Gamma_{1\pi}(x)$ denotes the section of $C \bigcup L$ bounded by $L_{1\pi}(x)$. $\Gamma_{1\pi}(x)$ satisfies Properties 1, 2 similarly to the ideal circle and line case previously studied. We would like to prove that $\Gamma_{1\pi}(x)$ also satisfies Property 3, and the weight function $n(s, x, \alpha)$ satisfies Properties 4 and 5. The idea is to demonstrate that the number of intersection points between $\Gamma_{1\pi}(x)$ and a plane $\Pi(x)$ passing through x in the ROI is at most three. If that is the case, then the weight distribution will be analogous to the one in the ideal circle and line problem.

The results follow if we show that the projection of the curve C on the detector is convex.

Definition 5 *Let $C \in \mathscr{C}$, and $y(s) \in C$.*

$\Omega = \{x | x = \lambda y(0) + (1 - \lambda) y(s), s \in [0, s_{max}]\}$ is the set of points located on all chords from the origin $y(0)$ to $y(s)$, a point on the curve, when the parameter $s \in [0, s_{max}]$.

Definition 6 *The region of interest (ROI) is any solid U whose projection $\hat{U}$ on the x-y plane is contained in Ω.*

Definition 7 *Let $C \in \mathscr{C}$, and x be a reconstruction point in the ROI. Consider the plane $\Pi(x)$ passing through x and the line L. The plane $\Pi(x)$ intersects the distorted circle at 2 points, $y(0)$ and y_C. Then the PI–line denoted by $L_{1\pi}(x)$ is defined to be the line segment containing the point x connecting $y_C(x)$ to the line L at some point $y_L(x)$.*

Lemma 8 *For every x in the ROI, $L_{1\pi}(x)$ is unique.*

PROOF: Let x be a point in the ROI. Because $C \in \mathscr{C}$, we can always find a plane $\Pi(x)$ passing through x and containing the line L. According to Definition 7, $\Pi(x)$ determines the $L_{1\pi}(x)$. To prove the uniqueness, let $L_{1\pi}(x)$ and $L_{1\pi}^{'}(x)$be two different Pi-lines. Let P_L be a vertical plane containing both the line L and the reconstruction point x. Then P_L intersects the circle C at y_C and $y_C^{'}$. Additionally, the corner of the circle and line $y(0)$ belongs to P_L. Now if we consider P_C the plane of the circle, then the points $y(0)$ and y_C belong to P_C. Also recall that the plane P_L contains the points $y(0)$, and y_C and $y_C^{'}$, so $y(0), y_C, y_C^{'}$ are contained in the intersection $P_C \cap P_L$. In other words, $y(0), y_C, y_C^{'}$ are not only on the curve C, but they are also colinear. This statement violates the fact that the curve C satisfies the convexity with respect to $y(0)$. Therefore $L_{1\pi}(x)$ must be unique. ■

Lemma 9 *Let $C \in \mathscr{C}$, and x be a point in the ROI. Then the following hold true:*

1. *There is no plane tangent to C in the interior of $\Gamma_{1\pi}(x)$ and passing through $L_{1\pi}(x)$.*

2. *There is no plane containing x, tangent to C in the interior of $\Gamma_{1\pi}(x)$, and passing through the corner $y(0)$ of the distorted circle and line.*

PROOF: *1.* Let x be a point in the ROI, P be a plane containing $L_{1\pi}(x)$ and tangent to the circle C at the point y_1. Then P contains y_C, y_1 and $\dot{y_1}$. If we let P_C be the plane of the circle, then P_C contains the points y_C and y_1. Thus the line passing through the points y_C and y_1 is the intersection of P_C with P. Also, note that P_C contains $\dot{y}_1$. Therefore, $\dot{y}_1 \in P_C \cap P = (y_C, y_1)$. In other words, the line passing through y_1 and y_C intersects the

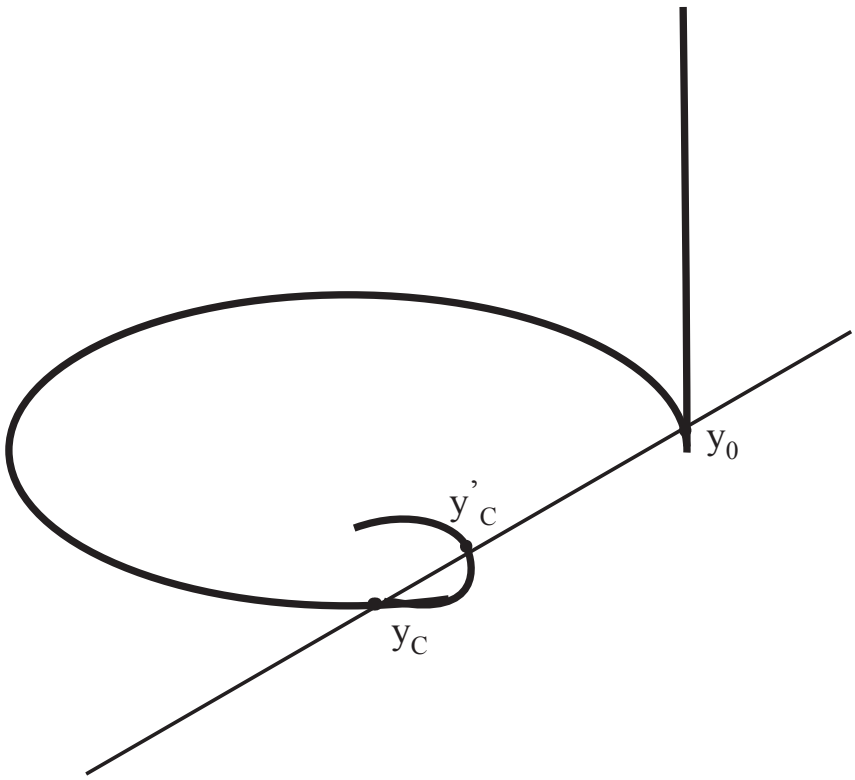

Figure 6.9: Violation of the Convexity w.r.t the origin $y(0)$

curve C at y_C and is also tangent to C at y_1, which contradicts Lemma 5.

2. This proof is analogous to the first one. Let P be a plane tangent to C at y_1 and containing the point $y(0)$. This allows us to say that the plane P contains $y(0), y_1$ and $\dot{y_1}$. Additionally, if we let P_C be the plane of the circle, then $y(0), y_1$ and $\dot{y_1}$ belong to P_C. Therefore, $y(0), y_1, \dot{y_1}$ are contained in the intersection $P \cap P_C$. In other words, the line passing through $y(0)$ and y_1 is tangent to the curve at y_1, which is contradictory to Lemma 5. ■

6.3.4 Projection on the Detector Plane DP(s)

Consider a point on the distorted circle. Assume $s \in I_2(x)$, then

$$y(s) = \Big(R(s)\cos(s), R(s)\sin(s), 0\Big), s \in [0, s_{max}] \tag{6.7}$$

where $R(s)$ is the variable radius of the circular trajectory such that $R(0)$ is the radius when $s = 0$. Let h be the height of the source position $y(s)$ above the plane of the circle. Recall that $\{x_1, x_2, x_3\}$ is the three dimensional coordinate system. Project x and C on the detector plane $DP(s)$, which is assumed to contains the x_3–axis. In addition, $DP(s)$ is perpendicular to the shortest line segment connecting $y(s)$ and the x_3-axis. Let $(u(s), w(s))$ be the coordinates of a point on the detector $DP(s)$ originated at $(0, 0, h)$.

Lemma 10 *The coordinates* $\Big(u(s), w(s)\Big)$ *of the projected source trajectory* $y(s)$, $s \in (0, s_{max}]$, *satisfy the following :*

$$u(s) = \frac{R(0)R(s)sin(s)}{R(0) - R(s)\cos(s)}, \tag{6.8}$$

$$w(s) = \frac{-hR(0)}{R(0) - R(s)\cos(s)} \tag{6.9}$$

PROOF: Let $y(s)$ be a point on C, $s \in (0, s_{max}]$, and let $(u(s), w(s))$ be its projection on $DP(s)$. Then we have the following three equations:

$$\begin{aligned} \lambda R(s)\cos(s) + (1-\lambda)R(0) &= 0 \\ \lambda R(s)\sin(s) + (1-\lambda)\cdot 0 &= u(s) \\ \lambda 0 + (1-\lambda)h &= w(s) + h \end{aligned} \tag{6.10}$$

One can solve for λ, substitute it into Equation 6.10, and obtain the following:

$$\begin{aligned} \lambda(s) &= R(0)/(R(0) - R(s)\cos(s)) \\ u(s) &= \lambda R(s)\sin(s) = \frac{R(0)R(s)\sin(s)}{R(0) - R(s)\cos(s)} \\ w(s) &= -\lambda h = \frac{-hR(0)}{R(0) - R(s)\cos(s)} \end{aligned} \tag{6.11}$$

■

Lemma 11 *Let $C \in \mathscr{C}$. Let $y(s) \in C, s \in (0, s_{max}]$, and $u(s)$ be the horizontal coordinate of its projection on the detector plane $DP(s_0)$, $s_0 \in I_1$. Then for every $y(s)$ on C, $\dot{u}(s) < 0$.*

PROOF: Let $y(s)$ be a point on the curve C, and let $u(s)$ be the horizontal coordinate of the projection of $y(s)$ on the detector plane $DP(s)$. First, observe that a simple computation allows us to write $\dot{u}(s)$, the derivative w.r.t. s of $u(s)$ defined in Lemma 10, as

$$\dot{u}(s) = \frac{\dot{y}(s) \times \Big(y(s) - y(0)\Big) \cdot e_3}{\Big(R(0) - R(s)\cos(s)\Big)^2} \tag{6.12}$$

where e_3 is the unit vector of the third component in the $\{x_1, x_2, x_3\}$ coordinate system. By Lemma 7, $(R(0) - R(s)\cos(s))^2 > 0$, and by Lemma 5, $\dot{y}(s) \times (y(s) - y(0)) \cdot e_3 \neq 0$, so

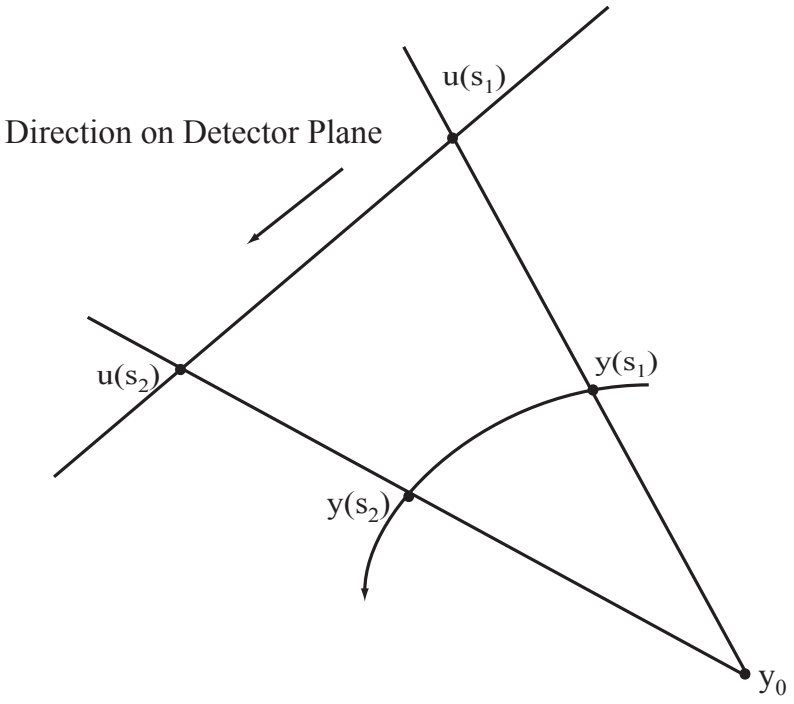

Figure 6.10: Illustration of Lemma 11

$\dot{u}(s) \neq 0$. Therefore, in order to prove that $\dot{u}(s) < 0$, for all s in $(0, s_{max}]$, it suffices to show that $\dot{u}(s) < 0$ when $s \to 0$. Also, note that showing $\dot{u}(s) < 0$ is equivalent to showing that $\dot{y}(s) \times (y(s) - y(0)) \cdot e_3 < 0$.

Let us expand $y(s)$ around $s = 0$, then

$$y(s) = y(0) + \dot{y}(0)s + O(s^2), s \to 0$$

and

$$\dot{y}(s) = \dot{y}(0) + \ddot{y}(0)s + O(s^2), s \to 0.$$

Thus

$$\begin{aligned}
\dot{y}(s) \times (y(s) - y(0)) \cdot e_3 &= \ddot{y}(0) \times \dot{y}(0)s^2 \cdot e_3 + O(s^3),\ s \to 0 \\
&= \Big(\ddot{y}(0) \times \dot{y}(0)s^2\Big) \cdot e_3 + O(s^3),\ s \to 0 \\
&= \Big(\ddot{y}(0) \times \dot{y}(0)s\Big) \cdot e_3 + O(s),\ s \to 0 \\
&= -\kappa(0)|\dot{y}(0)|^3 + O(s),\ s \to 0 \qquad (6.13)
\end{aligned}$$

where $\kappa(0) > 0$ is the curvature at $s = 0$. This implies that $\dot{u}(s) < 0$ as $s \to 0$. Therefore, $\dot{u}(s) < 0$ for all s in $(0, s_{max}]$. ■

Lemma 12 *Let (u(s), w(s)) be the projection of the source position y(s) on the detector plane $DP(s_0), s_0 \in I_1$. Then $\frac{d^2w}{du^2} < 0$.*

PROOF: Let $y(s)$ be a source position on the curve C. Then $y(s) = \Big(\alpha(s), \beta(s), 0\Big)$, where $\alpha(s) = R(s)\cos(s), \beta(s) = R(s)\sin(s)$. If $(u(s), w(s))$ is the projection of $y(s)$ on $DP(s)$,

then the second derivative is defined as follows,

$$\frac{d^2w}{du^2} = \frac{1}{\dot{u}(s)}\frac{d}{ds}\Big(\frac{\dot{w}(s)}{\dot{u}(s)}\Big). \tag{6.14}$$

Also for every s in $[0, s_{max}]$, the curvature is given by the formula below,

$$\kappa(s) = \frac{\dot{\alpha}(s)\ddot{\beta}(s) - \dot{\beta}(s)\ddot{\alpha}(s)}{\Big(\dot{\alpha}^2(s) + \dot{\beta}^2(s)\Big)^{3/2}}. \tag{6.15}$$

After some computations, Equation 6.15 can be reformulated in the following manner,

$$\kappa(s) = \frac{-\ddot{R}(s)R(s) + 2R(s)\dot{R}^2(s) + R^2(s)}{\Big(\dot{R}^2(s) + R^2(s)\Big)^{3/2}}. \tag{6.16}$$

By using Equation 6.16, the expression of the second derivative in terms of the curvature $\kappa(s)$ is derived below,

$$\frac{d^2w}{du^2} = \frac{C(s)\kappa(s)\Big(R(0) - R(s)\cos(s)\Big)}{\dot{u}(s)}, \tag{6.17}$$

where

$$C(s) = \frac{\Big(h\dot{R}^2(s) + R^2(s)\Big)^{3/2}}{\Big(\dot{R}(s)\sin(s) + R(s)\cos(s) - R^2\Big)^2} > 0. \tag{6.18}$$

Since $\dot{u}(s) < 0,\ R(0) - R(s)\cos(s) > 0$, and $\kappa(s) > 0$, then $\frac{d^2w}{du^2} < 0$. ■

Lemma 13 *The projection of the curve C on the detector plane $DP(s)$ is a convex curve.*

PROOF: The projection of the curve C on the detector plane $DP(s)$ is convex because for every s, $\dot{u}(s) < 0$ and $\frac{d^2w}{du^2} < 0$. ■

Conclusion: The conditions that we just derived state that the trajectory is not too exotic. In other words, we have proven that any plane passing through a reconstruction

point x in the ROI cannot intersect the curve C at more than 3 IPs. The distortions on the circle do not violate the number of intersection points (3 IPs at most) referred to in the ideal circle and line case. Consequently, the weight distribution remains the same, and a description of the weight function $n(s, x, \alpha)$ is summarized in Table 6.1 below.

6.4 Weight Distribution and Inversion Theorem

Table 6.1: Definition of the Weight Function $n(s, x, \alpha)$

Case	Weight Function $n(s, x, \alpha)$
1IP $s_1 \in I_1(x)$	$n(s_1, x, \alpha) = 1$
1IP $s_1 \in I_2(x)$	$n(s_1, x, \alpha) = 1$
3 IPs $s_1 \in I_1(x)$	$n(s_1, x, \alpha) = -1$
$s_2, s_3 \in I_2(x)$	$n(s_k, x, \alpha) = 1, k = 1, 2$

We have shown that our curve satisfies Properties $1 - 5$, so we can use Katsevich's inversion formula for the ideal circle and line case. The inversion formula is stated below.

Theorem 5 *Let $C \in \mathscr{C}$. For $f \in C_0^\infty(U)$,*

$$f(x) = -\frac{1}{2\pi^2} \int_{I_k(x)} \sum_{k=1}^{2} \frac{\delta_k(s, x)}{|x - y(s)|} \int_0^{2\pi} \frac{\partial}{\partial q} g(y(q), \Theta_k(s, x, \gamma))|_{q=s} \frac{d\gamma}{\sin \gamma} ds,$$

where

$$\Theta(s, x, \gamma) := \cos \gamma \beta(s, x) + \sin \gamma e_k(s, x), e_k(s, x) := \beta(s, x) \times u_k(s, x), \tag{6.19}$$

and δ_k is defined as follows:

$$\delta_1(s, x) = -\text{sgn}(u_1(s, x) \cdot \dot{y}(s)), \ s \in I_1(x); \ \delta_2(s, x) = 1, \ s \in I_2(x). \tag{6.20}$$

For completeness purposes, some numerical experiments are performed in order to demonstrate good image quality. The details of the implementation are mentioned in the next chapter.

CHAPTER SEVEN: THE ALGORITHM AND ITS IMPLEMENTATION

7.1 Description of the Cone Beam (CB) Measurements

A general description of the cone beam (CB) projections is first reviewed. Then for practical purposes, a description of the projections specific to the flat detector geometry is given. Such a description is highly convenient for the development of an efficient reconstruction algorithm.

The x-ray attenuation coefficient of the three dimensional object to be reconstructed is denoted by $f(\bar{x})$, where $\bar{x} \in R^3$. In what follows, f is assumed to be zero outside of the cylinder $x^2 + y^2 < r_0^2$, for $r_0 < R(0)$.

7.1.1 General Formulation

The cone beam (CB) is defined to be the set of all line integrals diverging from a given point in space often referred to as vertex. In computed tomography (CT), the vertex represents the point from which the x-ray are emanating. The CB projections are assumed to be known for every vertex point $y(s)$ on the trajectory. Below is the definition of the vertex point in our case

$$y(s) = (R(s)\cos(s), R(s)\sin(s), h). \tag{7.1}$$

Note that in order to make the x-ray source move along the circle, we let $h = 0$ and allow s to vary from 0 to a certain maximum scan angle denoted by s_{max}. It is also important to

mention that the maximum scan angle depends on the size of the region of interest (ROI). If the source is on the line then the parameter s is set to zero, while h varies along the line. For the purposes of the implementation, we consider the following smooth radius function

$$R(s) = R(0) - \frac{1}{2}\epsilon s^2, \tag{7.2}$$

where $R(0)$ is the radius of the circle when $s = 0$ and ϵ is a positive distortion parameter. Notice that if $\epsilon = 0$, we are in the case of the ideal circle and line trajectory.

In can be shown that the curvature $\kappa(s)$ remains positive with such a choice of $R(s)$. Indeed, if $R(s)$ is defined as in Equation 7.2, then

$$\dot{R}(s) = -\epsilon s, \qquad \ddot{R}(s) = -\epsilon. \tag{7.3}$$

By substituting Equation 7.3 into Equation 6.16, we obtain,

$$\kappa(s) = \frac{\epsilon R(s) + 2\epsilon^2 s^2 + R^2(s)}{\Big(\epsilon^2 s^2 + R^2(s)\Big)^{3/2}}, \tag{7.4}$$

which is positive since ϵ and the radius function $R(s)$ are both positive. Figure 7.1 gives a comparison between the ideal circle and the distorted circle for $R(0) = 570$ and $\epsilon = 5.0$. The graph shows that the curve satisfies the conditions of Definition 4.

7.1.2 Flat Detector Geometry

As introduced in Chapter 3, the CB projection g is a function of the source s, and the detector coordinates u and w. Therefore, to better describe the function, it is useful to

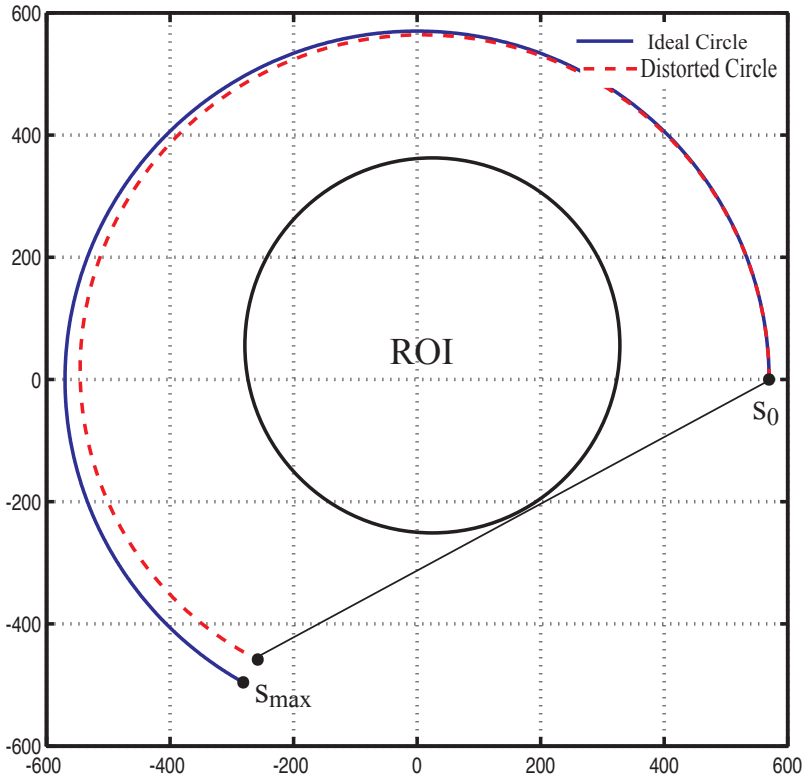

Figure 7.1: Ideal and Distorted Circle

introduce the following unit vectors for u and w respectively:

$$\begin{aligned} e_u(s) &= [-\sin(s), \cos(s), 0], \\ e_v(s) &= [-\cos(s), -\sin(s), 0], \\ e_w(s) &= [0, 0, 1]. \end{aligned} \tag{7.5}$$

The CB data is measured using a flat panel of detectors parallel to the x_3-axis and changing according to the source position. The detector plane is consequently perpendicular to the unit vector $e_v(s)$.

The detector is composed of rows and columns, which are respectively parallel to e_u and e_w. N_{row} and N_{col} respectively denotes the number of detector rows and columns. The center of the virtual detector is located at $(u = 0, w = 0)$. It is finally assumed that the distance between the detector and the source position is $R(s)$ because of the distortions on the circle. Using this geometry, the CB appears as a function $g(s, u, w)$ such that

$$g(s, u, w) = g(s, \theta), \tag{7.6}$$

with

$$\theta = \frac{ue_u(s) + R(s)e_v(s) + we_w(s)}{\sqrt{u^2 + w^2 + R^2(s)}}. \tag{7.7}$$

Also note that conversely, for a given direction θ pointing towards the detector, we have

$$g(s, \theta) = g(s, u, w), \tag{7.8}$$

where

$$u = R(s)\frac{\theta \cdot e_u}{\theta \cdot e_v} \qquad w = R(s)\frac{\theta \cdot e_w}{\theta \cdot_v}, \tag{7.9}$$

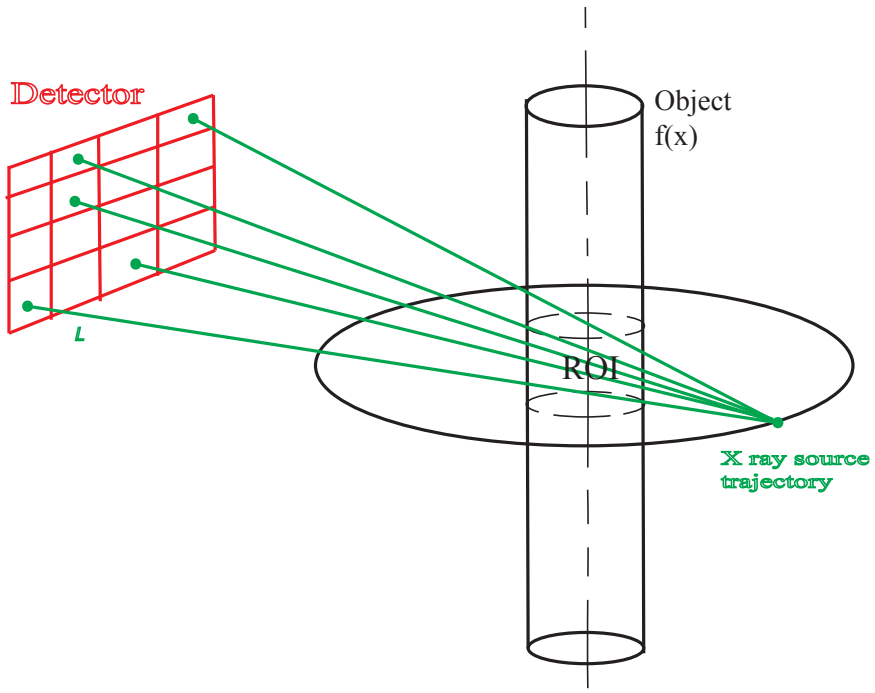

Figure 7.2: Flat Detector Geometry

7.2 Katsevich Formula

This section gives a description of the steps involved in the CB reconstruction. According to [1], for every x in the ROI, the three dimensional function $f(x)$ is reconstructed using CB backprojections over the segment of the curve (circle in our case) joining the two extremities of the Pi-line $L_{1\pi}(x)$ passing through x. The reconstruction formula is

$$f(\bar{x}) = -\frac{1}{2\pi}\int_{s_b(\bar{x})}^{s_t(\bar{x})} ds \frac{1}{||\bar{x}-y(s)||} g^F\Big(s, \frac{\bar{x}-y(s)}{||\bar{x}-y(s)||}\Big), \tag{7.10}$$

$s_b(\bar{x}), s_t(\bar{x})$, are the endpoints of $L_{1\pi}(x)$ such that $s_b(\bar{x}) < s_t(\bar{x})$. $g^F(s,\theta)$ is referred to as filtered data. In order to obtain $g^F(s,\theta)$, we first need to compute the derivative of the CB $g(s,\theta)$ with respect to s at a constant direction θ,

$$g^{'}(s,\theta) = \lim_{\epsilon \to 0} \frac{g(s+\epsilon,\theta) - g(s,\theta)}{\epsilon}. \tag{7.11}$$

Now $g'(s,\theta)$ is known, we can compute $g^F(s,\theta)$ according to the formula below,

$$g^F(s,\theta) = \int_0^{2\pi} g^{'}(y(s), \Theta_k(s,x,\gamma)) h_H(\sin\gamma) d\gamma, \tag{7.12}$$

where $\Theta_k(s,x,\gamma)$ was previously defined in 6.19 and h_H is the kernel of the Hilbert transform that is, $h_H(s) = 1/\pi s$.

As a remark, the computation of $g^F(s,\theta)$ in Equation 7.12 is called filtering, and the step involving the calculation of the integral over the segment $[s_b(\bar{x}), s_t(\bar{x})]$ in Equation 7.10 is referred to as backprojection. In other words, it follows from the formula in 7.10 that the reconstruction is achieved in two steps which are: filtering and backprojection.

7.2.1 Filtering

Derivative at a Constant Direction: Use the CB $g(s,u,w)$ to compute $g_1(s,u,w)$ such that $g_1(s,u,w) = g^{'}(s,\theta)$, where θ is given by Equation 7.7, and $g^{'}(s,\theta)$ is the derivative of the CB g with respect to s at a constant direction as defined in Equation 7.11.

Length Correction: Compute

$$g_2(s,u,w) = \frac{R(s)\cdot g_1(s,u,w)}{\sqrt{u^2+w^2+R^2(s)}}. \tag{7.13}$$

1 D Hilbert Transform in u: Compute

$$g^F(s,u,w) = \int_{-\infty}^{\infty} h_H(u-u^{'})g_2(s,u,u^{'})du^{'}, \tag{7.14}$$

where h_H is the kernel of the Hilbert transform that is, $h_H(s) = 1/\pi s$.

7.2.2 Backprojection

The filtered projection $g^F(s,u,w)$ is backprojected in order to build the three dimensional function f at each point $\bar{x} = (x_1,x_2,x_3)$ in the ROI according to the formula below,

$$f(\bar{x}) = -\frac{1}{2\pi}\int_{s_b(\bar{x})}^{s_t(\bar{x})} \frac{1}{v^*} g^F\Big(s,u^*(s,\bar{x}),w^*(s,\bar{x})\Big)ds, \tag{7.15}$$

where

$$v^*(s,x) = R(s) - x_1\cos(s) - x_2\sin(s), \tag{7.16}$$

$$u^*(s,x) = \frac{R(s)}{v^*(s,x)}(-x_1\sin(s) + x_2\cos(s)), \tag{7.17}$$

$$w^*(s,x) = \frac{R(s)}{v^*}(x_3). \tag{7.18}$$

7.3 Numerical Implementation Strategies

The steps of the numerical implementation of the Katsevich inversion formula on a flat detector geometry are originally described in [7]. In what follows, it is assumed that the CB $g(s,\theta)$ is sampled at,

$$\begin{aligned} s_k &= k\Delta s, \Delta s = 2\pi/N_s, \\ u_i &= (i-(N_{col}-1)/2)du, \\ w_j &= (j-(N_{row}-1)/2)dw. \end{aligned} \tag{7.19}$$

where du, dw, and N_s are respectively the horizontal, vertical, and the number of source positions. The available CB data are given by $g(s_k,u_i,w_j)$ where $k=0,...,N_s-2$, $i=0,...,N_{col}-2$, $j=0,...,N_{row}-2$.

Since our source trajectory consists of an incomplete circle and a line segment, then two cases will be considered for some of the steps involved in the numerical implementation.

7.3.1 Filtering

Derivative at a Constant Direction: The idea is to use $g(s_k,u_i,w_j)$ to compute samples of $g_1(s,u,w)$ such that $g_1(s,u,w)=g^{'}(s,\theta)$. By applying the chain rule to $g(s,u,w)$, and by using the relation in Equation 7.6, we obtain

$$g_1(s,u,w)=\Big(\frac{\partial g}{\partial s}+\frac{\partial g}{\partial u}\frac{\partial u}{\partial s}+\frac{\partial g}{\partial w}\frac{\partial w}{\partial s}\Big)(s,u,w). \tag{7.20}$$

Using Equation 7.9, for u and w yields

$$g_1(s,u,w) = \Big(\frac{\partial g}{\partial s}+\frac{\dot{R}(s)u+R^2(s)+u^2}{R^2(s)}\frac{\partial g}{\partial u}+\frac{\dot{R}(s)w+uw}{R(s)}\frac{\partial g}{\partial w}\Big)(s,u,w). \tag{7.21}$$

If the source position is on the circle, then from the last equation, the derivative $g_1(s,u,w)$ is numerically computed for $k=0,...,N_s-2$, $i=0,...,N_{col}-2$, $j=0,...,N_{row}-2$ as follows:

$$g_1(s_{k+1/2,},u_{i+1/2},w_{j+1/2}) \simeq \sum_{I=i}^{i+1}\sum_{J=j}^{j+1}\frac{g(s_{k+1},u_I,w_J)-g(s_k,u_I,w_J)}{4\Delta s} \tag{7.22}$$

$$+ \quad a_1(s)*\sum_{K=k}^{k+1}\sum_{J=j}^{j+1}\frac{g(s_k,u_{i+1},w_J)-g(s_k,u_i,w_J)}{4du} \tag{7.23}$$

$$+ \quad a_2(s)*\sum_{K=k}^{k+1}\sum_{J=j}^{j+1}\frac{g(s_k,u_I,w_{j+1})-g(s_k,u_I,w_j)}{4dw} \tag{7.24}$$

where

$$\begin{aligned} a_1(s) &= \frac{\dot{R}(s)u(s)+R^2(s)+u^2(s)}{R^2(s)}, \\ a_2(s) &= \frac{\dot{R}(s)w(s)+u(s)w(s)}{R(s)}. \end{aligned} \tag{7.25}$$

If the source is on the line, then for a fixed θ, the finite-difference derivative of the CB has the numerical expression below:

$$g_1(s_{k+1/2,},u_i,w_j) = \frac{g_1(s_{k+1,},u_i,w_j)-g_1(s_{k,},u_i,w_j)}{4\Delta s} \tag{7.26}$$

Length Correction: Regardless of the location of the source position, we use $g_1(s_{k+1/2},u_{i+1/2},w_{j+1/2})$ to compute,

$$g_2(s_{k+1/2},u_{i+1/2},w_{j+1/2}) = \frac{R(s)\cdot g_1(s_{k+1/2},u_{i+1/2},w_{j+1/2})}{\sqrt{u_{i+1/2}^2+w_{j+1/2}^2+R^2(s)}}. \tag{7.27}$$

1 D Hilbert Transform in u: The convolution in (7.14) can be efficiently implemented by taking the Fourier transform of g_2, multiply it by the Fourier transform of the Hilbert Kernel, and then by taking the inverse Fourier transform. This is justified by the following

property below,

$$h \otimes g = F^{-1}(Fh \cdot Fg) \tag{7.28}$$

where F represents the Fourier transform. Note that from a computational standpoint, some care must be taken to avoid aliasing. In order to account for aliasing, the function $g_2(s, u, w)$ evaluated at half pixels, say $g_2(s_{k+1/2}, u_{i+1/2}, w_{j+1/2})$ is zero-padded before applying the Fast Fourier Transform (FFT). Also, the fourier transform of the Hilbert kernel is taken over the interval $[-A/2, A/2]$, where A is the size of the sampled signal.

If the source is on the circle, then the process described above is done along the detector rows (see Figure 7.3).

If the source is located on the line, the 1 D Hilbert tranform in u is done as follows. Let $\hat{C}$ be the projection of the curve C on the detector plane $DP(s)$. By Lemma 13, $\hat{C}$ is a convex curve. Let $(R(0), 0, h)$ be a source position on the line segment, and $(0, H)$ be the tip of the pencil as depicted in Figure 7.4. Then the projection of the tip of the pencil $(0, H)$ from the point $(R(0), 0, h)$ on $DP(h)$ is $(0, H - h)$. Let T_{min} be the line passing through the point $(0, H - h)$ and tangent to $\hat{C}$ at some point whose parameter is denoted by q_{min}. Analogously, q_{max} is defined to be the parameter of the intersection point between the line T_{max} tangent to $\hat{C}$ and the left boundary of the cylinder. Now, choose a parameter q_0 such that $q_{min} < q_0 < q_{max}$, and let T_{q_0} be the tangent to $\hat{C}$ at q_0. We find the intersections $\{u_i, i\}$ between the detector columns and T_{q_0}. Let u_{j_0} be an intersection point between T_{q_0} and a detector column, and w_{j_0} be its corresponding vertical coordinate. Since $u_j < u_{j_0} < u_{j+1}$, $w_i < w_{j_0} < u_{i+1}$, and $g_2(u_{j_0}, w_i)$, $g_2(u_{j_0}, w_{i+1})$ are known, we use linear interpolation to calculate $g_2(u_{j_0}, w_{j_0})$. We then obtain the following set $\{g_2(u_{j_0}, w_{j_0}), i_0 = 1, ..., N_c - 2\}$ on

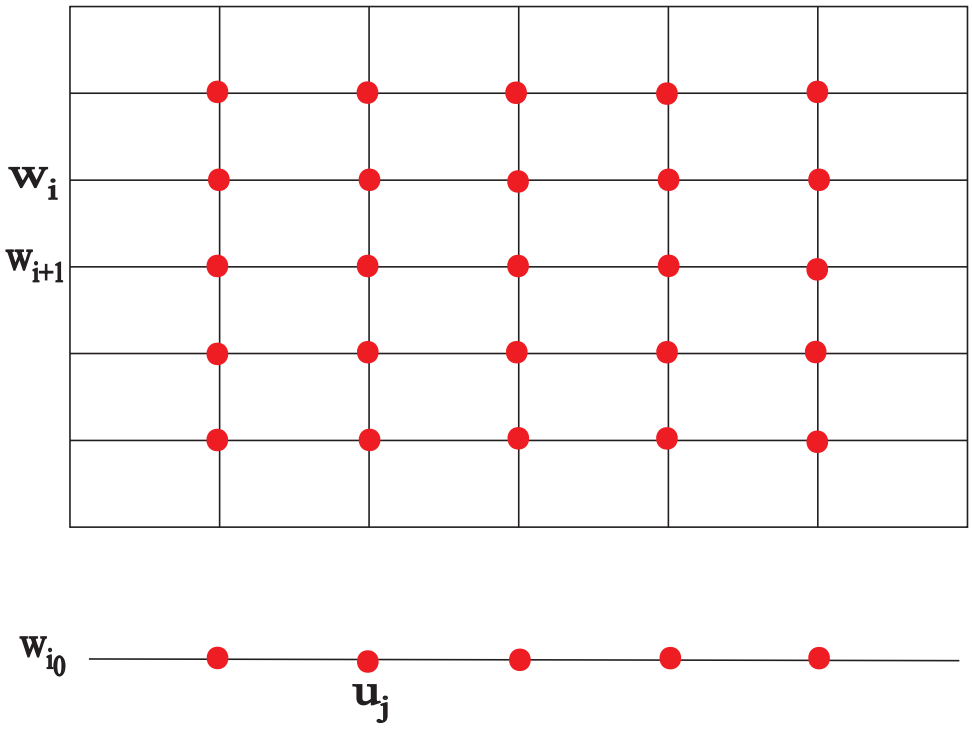

Figure 7.3: Filtering when the source is on the Circle

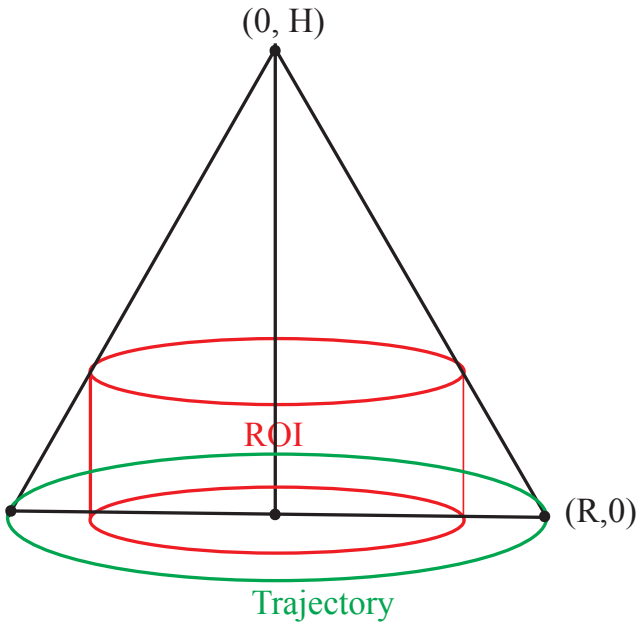

Figure 7.4: Illustration of the Height of the Cylindrical ROI

which we perform the 1-D Hilbert transform. Figure 7.6 gives an illustration of the process. By repeating the process for N_q parameters between q_{min} and q_{max}, we recover an N_q by N_{col} matrix which will be used for backprojection. See Figure 7.5.

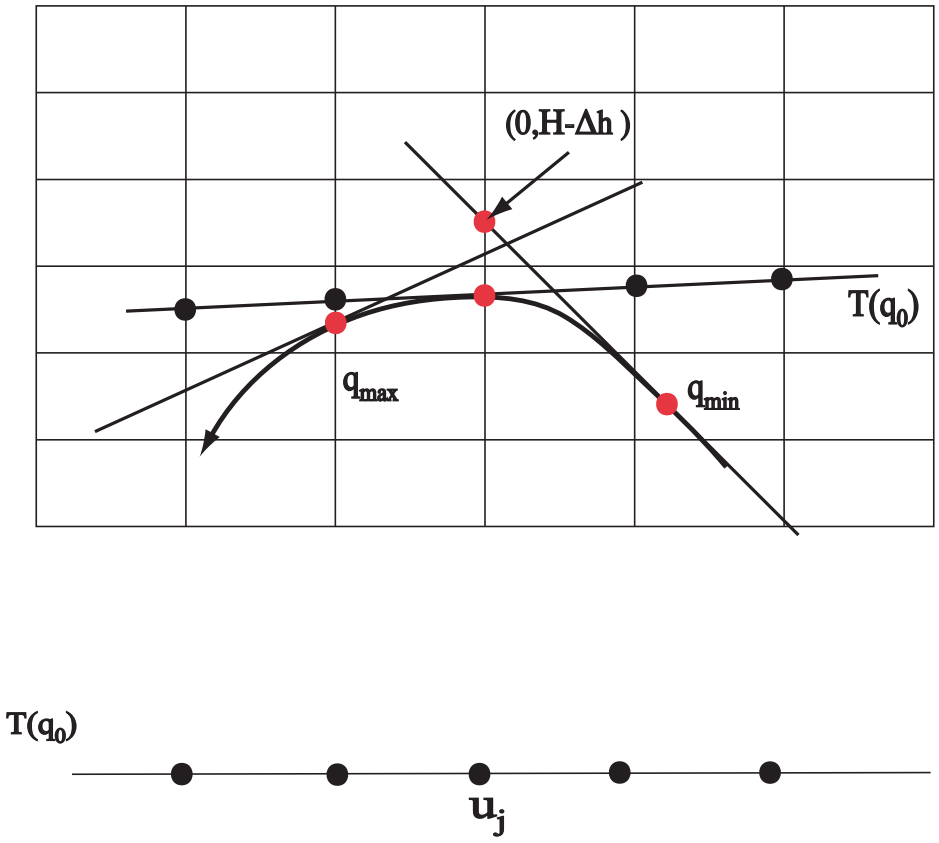

Figure 7.5: Filtering when the source is on the Line

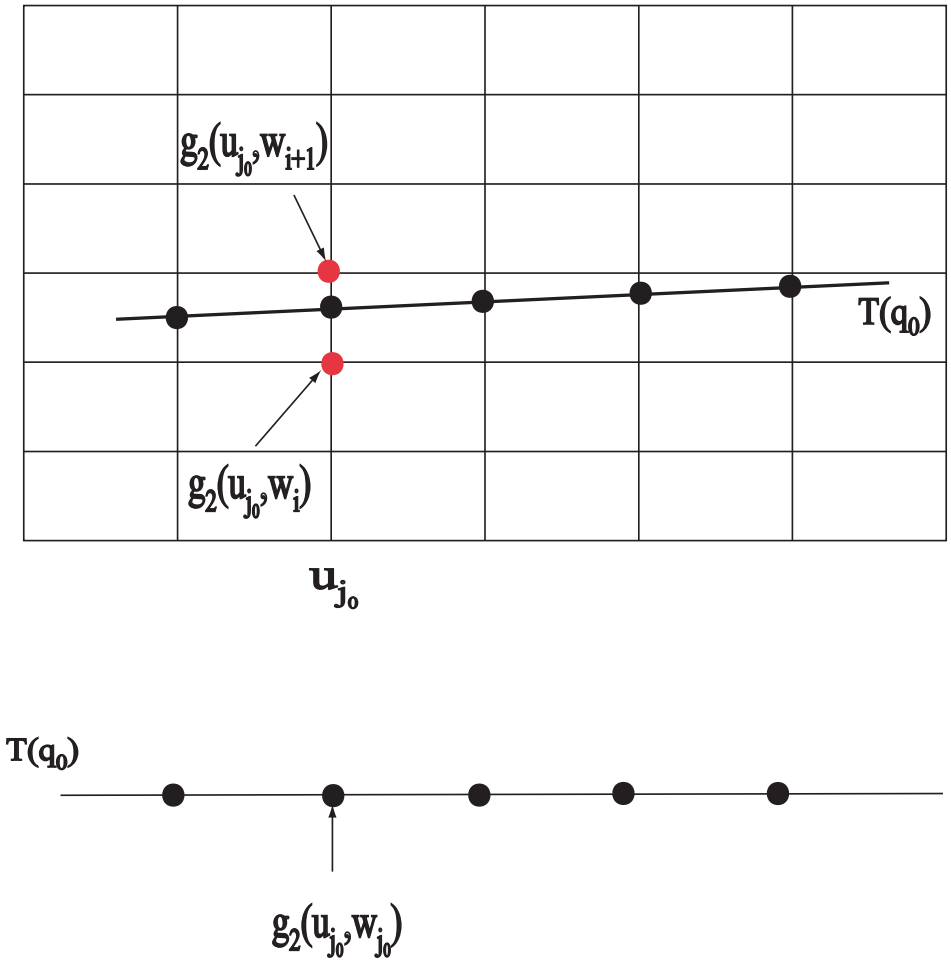

Figure 7.6: Filtering when the source is on the Line (Interpolation)

7.3.2 Backprojection

Let $\bar{x}$ be a point in the ROI, and its projection (u^*, w^*) be on the detector plane. The filtered projection $g^F(s, u, w)$ is backprojected according to Equation 7.15 in order to recover the three dimensional function f for every $\bar{x}$ in the ROI.

Source on the Circle Once the point (u^*, w^*) is located on the grid i.e $u_j < u^* < u_{j+1}$ and $w_i < w^* < w_{i+1}$, bilinear interpolation is performed using the discretized function $g_3(s, u, w)$ in order to obtain the corresponding backprojected $g^F(s, u^*, w^*)$.

Source on the Line For each point $\bar{x}$ in the ROI, compute the projection (u^*, w^*) on the detector $DP(s)$ according to Equation 7.16. Assume (u^*, w^*) is above the projected curve $\hat{C}$, and $u_i < u^* < u_{i+1}$, use linear interpolation to find the corresponding parameter s^* such that $s_i < s^* < s_{i+1}$. Next, calculate the parameter q^* such that the line passing through (u^*, w^*) is tangent to the projected curve $\hat{C}$. Now that q^* is computed, and located on the $u - q$ grid, we use the discretized values of the function $g_3(s, u, w)$ and bilinear interpolation to compute the backprojected value $g^F(q^*, u^*)$. See Figure 7.8 as an illustration.

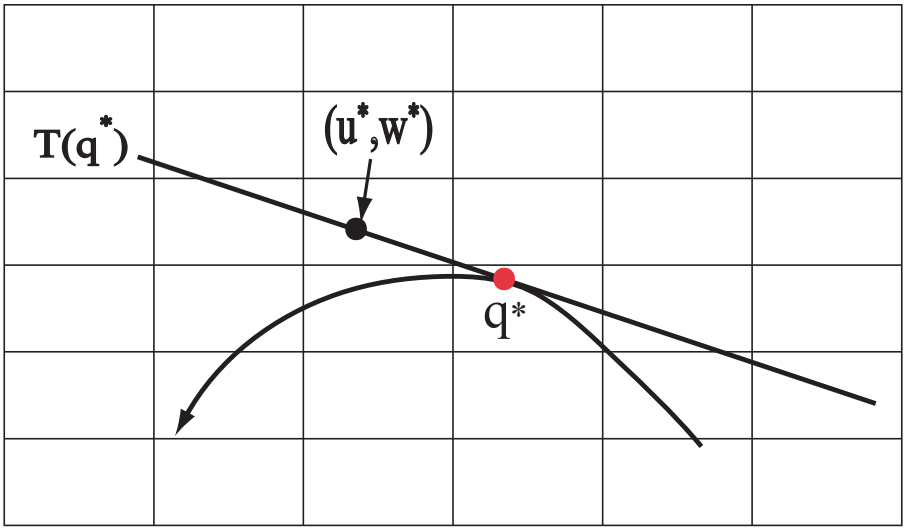

Figure 7.7: Backprojection

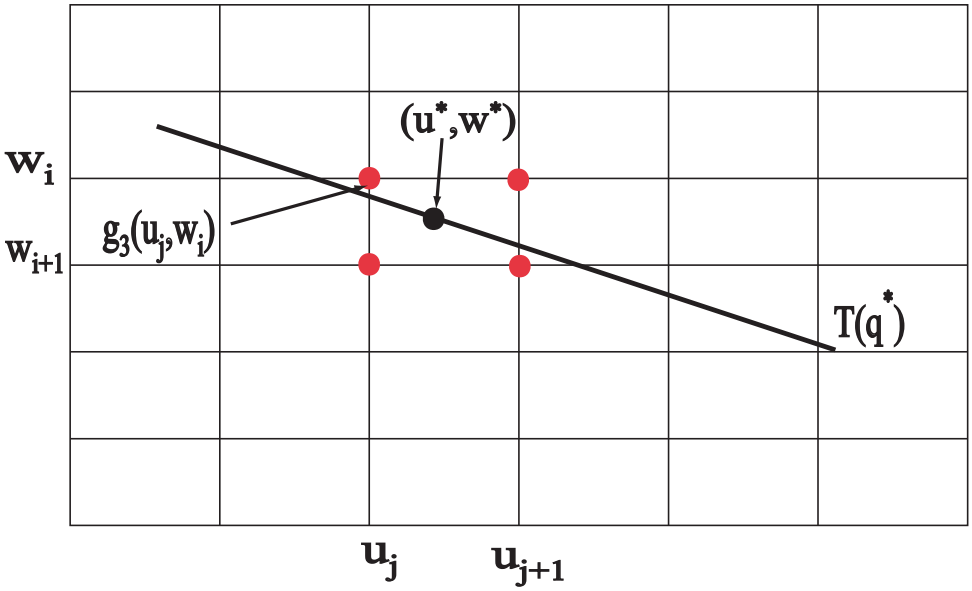

Figure 7.8: Bilinear Interpolation prior to Backprojection

CHAPTER EIGHT: NUMERICAL RESULTS

In this chapter, we first start with a brief definition of the Hounsfiled unit, and we discuss the numerical experiments that we conducted in order to test for good image quality.

The Hounsfield unit (HU) is a standardized and accepted measurement system for reporting and displaying reconstructed X-ray CT values. The HU was named after the British electro-engineer Sir. Godfrey N. Hounsfield who developed the first clinically useful CT machine. The system of units represents a transformation from the original linear attenuation coefficient into a system where water and air are assigned the values 0 and -1000 respectively. In other words, assume μ_w, μ_a, and μ are linear attenuation coefficients of water, air and an unknown substance, then the corresponding HU value is given by the equation below

$$HU = 1000\frac{\mu - \mu_w}{\mu_w - \mu_a}. \tag{8.1}$$

Therefore one (HU) corresponds to 0.1% of the attenuation coefficient difference between water and air, or we can say approximately 0.1% of the attenuation coefficient of water since the attenuation coefficient of air is nearly zero. Table 8.1 gives the HU of some common substances.

In order to test the proposed algorithm, we conducted some numerical experiments with the clock phantom which was originally described in[22]. The background cylinder was at 0 HU, the spheres were at 1000 HU, and the air at -1000 HU. Under the assumption that the plane of the circle is at $z = 0$, the phantom is shifted by $\Delta z = +20.0$. The purpose of this shift is to better illustrate how well the algorithm reconstructs cross-sections which

Table 8.1: HU of Some Common Substances

Substance	HU
Air	-1000
Water	0
Bone	≥ 400
Muscle	40
Fat	-120

are located away from the plane of the circle. The size of the image is 512 x 512, which corresponds to the following ROI $|x| \leq 250$ and $|y| \leq 250$. In order to make small artifacts visible, we introduce a highly compressed grey level window level and window width of $[1.0, 0.1d]$, for a density $d = 1$. Besides small numerical discretization artifacts, the quality of the reconstructed cross section is good.

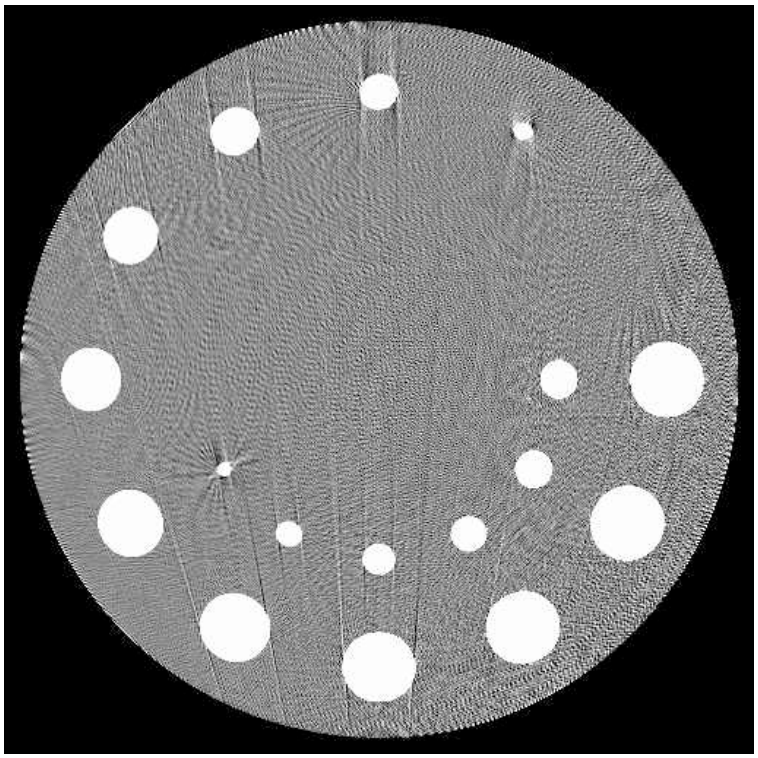

Figure 8.1: Cross section $z = 20$ mm through the reconstructed clock phantom. The region $|x| \leq 250$,$|y| \leq 250$ mm is show for a distortion parameter of $\epsilon = 5.0$

Table 8.2: Simulation and Reconstruction Parameters

Parameter	Value	Unit
Radius of the circle	570	mm
Distortion parameter ϵ	5.0	
Height of the line L	160	mm
Detector pixel size at isocenter	0.7	mm^2
Number of detector rows	551	
Number of detector columns	1001	
Number of source positions on the circle	600	
Number of source positions on the Line	160	
Number of FFT points	2048	
Number of filtering lines for source points	200	
Radius of the ROI	250	

LIST OF REFERENCES

[1] A.I.Katsevich. Image reconstruction for the circle and line trajectory. *Institute of Physics Publishing*, 49, 2004.

[2] A.Katsevich. A general scheme for reconstructing inversion algorithms for cone beam CT. *International Journal of Mathematics and Mathematical Sciences*, 2003, 2003.

[3] T. Aubin. *A Course in Differential Geometry, Graduate Studies in Mathematics Vol. 27.* American Mathematical Society, Rhodes Island, New York, 2001.

[4] M. Defrise and R. Clack. A cone-beam reconstruction algorithm using shift-variant filtering and cone-beam backprojection. *IEEE Trans. on Medical Imaging*, 13, 1994.

[5] M. Defrise, F. Noo, and H.Kudo. A solution to the long-object problem in helical cone-beam tomography . *Phys. Med. Biol.*, 45, 2000.

[6] F. Noo et al. Stable and efficient shift-variant algorithm for circle-plus-lines orbits in cone-beam CT Proc. Int. *Conf. on Image Processing*, 3, 1996.

[7] J. Pack F. Noo and D. Heuscher. Exact helical reconstruction using native cone-beam geometries. *Institute of Physics Publishing*, 48, 2003.

[8] D.V. Finch. Cone beam reconstruction with sources on a curve. *SIAM J. Appl. Math.*, 45, 1985.

[9] I. M. Gelfand and A. B. Goncharov. Recovery of a compactly supported function starting from its integrals over lines intersecting a given set of points in space. *Soviet Math. Dokl.*, 45, 1987.

[10] I.M. Gel'fand and G. E. Shilov. *Generalized Functions Volume I.* Academic Press, New York and London, 1964.

[11] P. Grangeat. Mathematical framework of cone–beam reconstruction via the first derivative of the Radon transform. *JCP*, 1497, 1991.

[12] A. Greenleaf and G. Uhlmann. Nonlocal inversion formulas for the X-ray trans- form. *Duke Math. J*, 58, 1989.

[13] H.K.Tuy. An inversion formula for cone-beam reconstruction. *SIAM J. Appl. Math.*, 43, 1983.

[14] A. Katsevich. Improved exact FBP algorithm for spiral CT, Preprint. *Math. Methods Appl. Sci*, 23, 2000.

[15] A. Katsevich. On quasi-local inversion of spiral CT data. *Math. Methods Appl. Sci*, 23, 2000.

[16] A. Katsevich. An inversion algorithm for Spiral CT. *Proceedings of the 2001 International Conference on Sampling Theory and Applications (A. I. Zayed, ed.) University of Central Florida*, 1, 2001.

[17] A. Katsevich. Theoretically exact filtered backprojection-type inversion algorithm for spiral CT. *SIAM J. Appl. Math.*, 62, 2002.

[18] A. Katsevich. Analysis of an exact inversion algorithm for spiral cone-beam CT. *Phys. Med. Biol.*, 47, 2002.

[19] A. Katsevich. A general scheme for constructing inversion algorithms for cone beam CT . *Int. J. Math. Sci.*, 21, 2003.

[20] H. Kudo and T. Saito. Derivation and implementation of a cone-beam reconstruction algorithm for non-planar orbits. *IEEE Trans. on Medical Imaging*, 13, 1994.

[21] F. Natterer. Recent developments in X-ray tomography, Tomography, Impedance Imaging, and Integral Geometry (South Hadley, Mass, 1993). *Lectures in Appl. Math., American Mathematical Society, Rhode Island*, 30, 1998.

[22] Turbell H Danielsson P-E. Helical cone beam tomography. *Int. J. Imaging Syst. Technol.*, 11, 2000.

[23] A.G. Ramm and A. I. Katsevich. *Radon Transform.* CRC, NYC, 1996.

[24] G.L. Zeng and G.T. Gullberg. A cone-beam tomography algorithm for orthogonal circle-and-line orbit. *Phys. Med.*, 37, 1992.